EUROPEAN ORGANIZATION FOR NUCLEAR RESEARCH

CERN/SPSC 74-3
SPSC/P 4
23.1.1974

PROPOSAL FOR A DETAILED STUDY OF HIGH-P_t EVENTS AT THE SPS

P. Baillon, G. Bizard, C. Bricman, Y. Déclais, R. Donald,
J. Duchon, D. Edwards, M. Ferro-Luzzi, B. French, B. Ghidini,
W. Kienzle, F. Lefebvres, P. Litchfield, L. Mandelli, F. Muller,
J.-M. Perreau, V. Picciarelli, J.P. Patry, J. Séguinot,
L. Tallone and T. Ypsilantis

BARI(*)-CAEN-CERN (NP/TC)-LIVERPOOL(+)-MILAN(*)

(*) Subject to approval by INFN

(+) Subject to approval by DNPL

TABLE OF CONTENTS

I. SUMMARY

It is the aim of the proposed experiment to study in full detail the properties of hadronic interactions giving rise to particles with large transverse momentum. An almost complete momentum analysis of the events is envisaged with emphasis on the identification of the charged particles ($3 < P_{lab} < 80$ GeV) in a large solid angle. This experiment will permit us to probe the nucleon structure down to distances of 0.04 fermi. We specifically concentrate on the following questions:

(i) Dependence of high P_t events on the incident particle ($\pi^{\pm}, K^{\pm}, p^{\pm}$)

(ii) Composition of the events as a function of P_t and the nature of the high P_t particle on which we trigger.

(iii) Do jet like correlations occur, suggestive of parton-parton scattering?

(iv) What is the jet cross section, multiplicity, composition and mass distribution?

(v) Do new massive objects exist such as e.g. heavy "fire balls", resonances, charmed particles, etc.?

The apparatus consists of a fast (MWPC's) magnetic vertex detector plus a field free forward lever arm composed of Čerenkov hodoscopes, sandwiched between drift chambers. At 150 GeV/c and with 10^7 incident particles per pulse we expect 12,000 events/day with $P_t > 3$ GeV/c (safety factor 0.5). The price tag is 4 MSF not including the magnet (1.5 MSF).

We plan to have the equipment ready for use in the H1 beam of the West Area at the start up of the SPS.

II. APPARATUS

The equipment we propose is shown in fig. 1. Our basic idea is to concentrate all the bending power at the vertex. The forward region is thus available for particle identification which we consider important; furthermore, it provides the necessary lever arm for measurement of fast forward particles. Here we describe the essential features of the spectrometer and triggering system.

1. Beam

We propose this experiment for the H1 beam in the West Area and to begin with a negative beam at 150 GeV/c. Particle intensities are given in Table 1. We plan to run at 10^7 incident particles per pulse. The direction of the incident particle will be determined by three small MWPC's in the beam upstream from the target. We are developping chambers with a wire spacing of ± 100μ and operating at high pressure. They will determine the incident particle transverse position in the H_2 target (30 cm in length) to < 100μ and the angle to < 0.1 mrad. leading to a transverse momentum error of < 15 MeV/c. The momentum of the selected particle will be determined to high precision by standard equipment provided by the beam group. Particle identification is done by a DISC Čerenkov counter.

2. Vertex Detector

For track measurement in the vertex detector we have chosen a fast multiwire proportional chamber system (MWPC); this choice is dictated by the presence of a strong magnetic field (∿ 17 kG) and the need for good spatial resolution in a region where the track density is highest. The configuration of the chambers has been studied with Monte Carlo simulation procedures so as to optimize the reconstruction capability and the accuracy.

This kind of chamber and geometry was chosen to satisfy certain criteria viz:

(a) to give accurate points in space so that pattern recognition can be done in space;

(b) to give sufficient points for presently working fast pattern recognition programs;

(c) to give reasonably efficient detection of multitrack events and large angle, low momentum particles (9% loss of tracks for peripheral interactions, 0.4% loss for high P_t type events) ;

(d) that the mechanical construction of the wire chambers is relatively straightforward;

(e) that the lateral dimensions are large enough to give $\delta P_t \lesssim 20$ MeV/c for tracks with $P_t < 1$ GeV/c and $P < 10$ GeV/c, which are reconstructed in the vertex detector;

(f) that $\Delta P/P < 2\%$ for tracks with $P < 10$ GeV/c.

The preferred configuration, shown in fig. 1, consists of one series of six modules (1 x 0.8 m^2 useful area) perpendicular to the beam and distributed over two metres downstream from the hydrogen target plus two series of four vertical modules each (0.6 x 0.8 m^2) on both sides of the target. Each forward module consists of one plane of vertical wires and two planes of inclined wires ($\pm 25^o$) with 2 mm wire spacing. Each side module consists of one plane of vertical wires, one plane of horizontal wires, and an additional plane of wires tilted by 5 degrees. There are a total of 16,000 wires inside the magnet. The spatial resolution per module is $\Delta X = \pm 350\mu$ and $\Delta Y = \pm 500\mu$. Charged particles with momentum $P < 10$ GeV/c are analysed with a precision of $\Delta P/P < 2\%$ and $\Delta P_t/P_t < 2\%$. The variation of the momentum resolution with P for various values of P_t is shown in fig. 2a. The effective mass resolution is $\Delta M = \pm 10$ MeV for a mass of 1 GeV (momentum 10 GeV/c) decaying into $\pi^+\pi^-$; $\Delta M/M$ versus P(M) for various masses is shown in fig. 2b.

3. Magnet

Our considerations are based on a magnetic bending power of 40 kG meter giving a transverse momentum kick of 1.2 GeV/c. A magnet similar to the "GOLIATH" magnet of Saclay(*) would suit our purposes; other magnets could of course be used, provided the gap dimensions are of the order of 2 x 2 m^2 by 1.2 height with a field not less than 15 kG.

4. Forward Lever Arm

Fast particles ($P \gtrsim 10$ GeV/c) emitted in the forward direction are momentum analyzed and identified in a system of three drift chambers(**) and four Čerenkov counter hodoscopes after the magnet. At $P_{inc} = 150$ GeV/c this system covers $0^\circ < \theta^* < 135^\circ$ in the c.m. and identifies $\pi^\pm$, $K^\pm$, $p^\pm$ as shown in fig. 3. For example, at $\theta^* = 90^\circ$ all particles are identified up to $P^* = 5$ GeV/c. Momentum analysis is done with the lever arm technique, the momentum resolution being given by the expression(***)

$$\frac{\Delta P}{P} = \frac{200\ P}{3\ B\ \ell} \left[(\delta_o/\ell)^2 + \delta_1^2 (1/\ell + 1/L)^2 + (\delta_3/L)^2 \right]^{\frac{1}{2}} \qquad (1)$$

where:

- P = particle momentum (GeV/c)
- B = magnetic field strenght (kG)
- ℓ = effective field length (m)
- L = distance between drift chambers 1 and 3
- δ_o = ± 100μ from incident beam chambers
- δ_1 = ± 300μ from drift chamber 1
- δ_3 = ± 700μ from drift chamber 3

} the drift chamber resolutions are optimized in order to give equal contributions in expression (1).

The drift chambers have 2 cm wire spacing. The required resolution is ± 300μ und ± 700μ for chambers 1 and 3 respectively. Each of the drift chambers consists of two vertical planes shifted by half the wire spacing,

---

(*) A copy of GOLIATH would be a useful general purpose magnet for SPS experiments. We have been in touch with the factory (ALSTHOM, at Belfort, France) who indicate a price of ∿ 1.5 MSF for an identical copy and a delivery time of 17 months due to the fact that the design and tooling already exists.

(**) Drift chamber 4 is used for redundancy in track reconstruction through C4 and M2.

(***) Drift chamber 2 between 1 and 3 does not add to the precision, but is

two horizontal planes again shifted by half the wire spacing and a crossed plane to remove geometrical ambiguities. Since all tracks of interest in these chambers are of high momentum, the particles are incident at an angle less than 20^{o} to the normal; hence two chambers are enough to resolve right-left ambiguities. For a particle of 50 GeV/c passing through the lever arm we expect a momentum resolution of $\Delta P/P = \pm 3\%$. The transverse momentum resolution $\Delta P_t/P_t$ is shown in fig. 4.

In a narrow forward cone ($\lesssim$ 50 mr), where particle density is highest ("forward jet") we back-up the drift chambers by three additional small MWPC's. This will allow us to detect the fastest particles which are separated from the beam by a distance of a few centimeters.

Identification of charged particles is achieved for $2 \lesssim P_{lab} \lesssim 80$ GeV/c by a system of four gas Čerenkov hodoscopes Č1 - Č4 at atmospheric pressure. Their characteristics are listed in Table 2 and shown in fig. 5.

In Table 2 the number N_o (cm^{-1}) which takes into account the photomultiplier efficiency and the mirror reflectivity for the accepted frequency interval, allows to calculate the total number of photoelectrons which is $N = N_o L \theta_C^2 = N_o L (1-1/\beta^2 n^2)$. A conventionally accepted value of N_o is 100 cm^{-1} as used e.g. for our counter Č1. In order to keep the counters Č2 - Č4 as short as possible and thus the Cerenkov light circle on the mirrors small for good hodoscoping we use the value of $N_o = 164$ cm^{-1} obtained for a new RCA photomultiplier in recent measurements of Yovanovitch et al.(*). Substantial further gains are possible by using special mirror coatings and wave shifters. Each counter is subdivided into a number of optical cells using elliptical mirrors so as to resolve in space the different tracks of a given multiparticle event. The mirrors are arranged laterally in one row above and one below the beam as shown in fig. 6. In addition, each Čerenkov counter contains, for trigger purposes, a ring of shorter mirrors covering the same solid angle as the trigger scintillators. Their light is reflected into separate photomultipliers (see figs 6 and 7) which are used in the trigger as described below.

(*) Nuclear Instr. and Methods 94 (1971) 477.

Detection of π^o's is intended at a later stage. Since the detector must be located behind the last Čerenkov counter (C4) and should also cover $\theta^* \lesssim 135^o$ it would be of large dimensions ($\sim 6 \times 6$ m^2). A lead glass array would therefore be quite expensive. We think to detect just the positions of the γ-rays coming from π^o decays by materialising them in a lead sheet backed by an additional wire chamber (dashed line in fig. 1). This could give considerable information at minimal expense and allow the selection of a subsamble of π^o-free events for fitting. However, the present apparatus is designed such that measurements on the charged particles alone gives enough precision in the transverse momentum balance to determine in most cases whether or not neutrals are present in the reaction.

5. Trigger

In the first stage of the experiment we plan to trigger on charged particles(*) with $P_t \gtrsim 3$ GeV/c, emitted at $80^o \lesssim \theta^* \lesssim 100^o$ in the c.m. The trigger acceptance is uniform in the azimuthal angle ϕ and covers a solid angle $\Delta\Omega = 2.2$ steradians. By displacing the trigger system we can explore different regions in θ^*. The basic aim of our trigger is the elimination of peripheral interactions by asking for a particle emited at a large lab angle and with large momentum. This is achieved by the combined requirement of a signal in the scintillation hodoscopes M1M2 and in the threshold Čerenkov counters.

The trigger selection is defined by:

(i) a coincidence in the beam telescope $S_1 S_2$;

(ii) a coincidence between two elements of the scintillation hodoscopes M_1 and M_2 located after the magnet (fig. 1). These hodoscopes are ring shaped and made up of vertical slabs of scintillators as shown in fig. 8. The slab width is 1 cm in M_1 and 2 cm in M_2. For particles of a given θ^* and P_{LAB} with

---

(*) We have chosen to trigger on charged particles for reasons of rate, cost and flexibility. We have also studied a π^o trigger which is in principle straight forward, were the leadglass counter available ($\sim$ 0.5 MSF per steradian). The stability and background rejection may be more difficult problems than for a charged trigger. Similarly

azimuthal angle ϕ a correlation exists between the lateral position y_1 in the counter hodoscope M, and the lateral position y_2 in the hodoscope M_2 (see fig. 9a), given by the equations

$$y_1 \doteqdot (L+\ell)\,\frac{\tan\theta^*/2}{\gamma c}\,\sin\phi + L\,\frac{\Delta}{P} \qquad (2)$$

$$y_2 \doteqdot (M+\ell)\,\frac{\tan\theta^*/2}{\gamma c}\,\sin\phi + M\,\frac{\Delta}{P}$$

Δ = transverse momentum kick given to a particle by the magnetic field (1.2 GeV/c for 40 kG meter).

ℓ,L,M are defined in fig. 9a.

When ℓ, θ^*, and Δ/P vary in their (small) allowed ranges there is a sharp y_1-y_2 correlation as shown in fig. 9b. A suitable coincidence requirement between elements of M_1 and M_2 allows us therefore to select the desired interval in θ^* and a lower cutoff in P_t (e.g. $P_t > 2.2$ GeV/c at $\theta^* = 80^\circ$ and $P_t > 3$ GeV/c at $\theta^* = 100^\circ$).

(iii) signals from the Čerenkov counters:

(a) C1 in fast coincidence with a ring of scintillators S_3 which match the trigger mirrors of C4 (description above). This condition requires an interaction in the target and makes sure that a particle has traversed the whole Čerenkov system;

(b) different types of particles are identified in the trigger by requiring C_i = (π = C1$\overline{\text{C2C3C4}}$) or (K = C1C2$\overline{\text{C3C4}}$) or (p = C1C2C3$\overline{\text{C4}}$). This establishes a threshold of $P^{\pi}_{lab} \simeq 18$ GeV/c (see Table 1).

Thus the full trigger condition is $(S_1S_2)(M_1M_2)(C1S_3)C_i$ (π,K,p). The time resolution is of the order of 30 nsec. and the random trigger rate should be less than $\sim$ 3%.

6. Trigger Acceptance and Background

In order to determine the precise acceptance of the trigger system we have generated a Monte Carlo sample of high P_t tracks ($P_t > 3$ GeV/c and $80^\circ < \theta^* < 100^\circ$) to determine the correlation Y_1 vs Y_2. This is shown in fig. 10a. The tracks were generated with a flat distribution in X_t and X_{11}. We then generated a complete sample of tracks over the full range of P_t and cos θ^* and looked at particles accepted by the matrix designed in accordance with fig. 10a. We found that 98% of the generated tracks with $P_t > 3$ GeV/c and $80^\circ < \theta^* < 100^\circ$ were accepted. In addition, however, a certain number of tracks of lower P_t and smaller θ^* were accepted. In fig. 10b we show the momentum distribution of the accepted tracks (note that $P_{lab} > 18$ GeV/c) and in fig. 10c the scatter plot of P_t vs. The projections on the θ^* and P_t axes are shown in figs 10d and 10e. Taking into account the steep rise of cross section with decreasing P_t we estimate that 20 times more events with $P_t < 3$ GeV/c will be accepted by the trigger system than events with $P_t > 3$ GeV/c. This rate can be handled by our data acquisition system and the events are not uninteresting.

In the "K trigger" $C_i = C1C2\overline{C4}$ and in the "p trigger" $C_i = C1\overline{C3}\overline{C4}$ and therefore π's between 5.2 + 17.0 GeV/c can simulate kaons and π's between 2.5 and 10.7 GeV/c and K's between 9.0 + 18.3 GeV/c can simulate protons. When we require the matrix correlation in addition to the Cerenkov trigger we find no contamination of π's in the K trigger and no contamination of π's or K's in the p trigger.

With an interaction rate of 5×10^5/sec in the target area and a maximum data acquisition rate of 100/sec we need a rejection of 5×10^3.

We have thought about the following possible sources of backgrounds which we are now evaluating:

(i) two particles from the same peripheral event, one in M_1 and the other in M_2, thus simulating a K or p trigger (this problem is not present for the pion trigger, since $P_{lab} > 18$ GeV/c is required by the Cerenkov system).

(ii) one particle through M_1 (M_2) and a background μ or a π° electron through M_2 (M_1);

(iii) an interaction in M_1 with a scattered secondary going through M_2 and thus simulating a K or p trigger.

If necessary, the information from the drift chambers between M_1 and M_2 may be used to reject these events by a slower on-line decision.

7. Rates

Rates have been estimated on the basis of a 10 nanobarn per steradian cross section, obtained by extrapolating to our c.m. energy ($\sqrt{s}$ = 16.8 GeV) the cross section integrated from 3 to 5 GeV/c (per π of one charge) of the Strasbourg-Saclay Collaboration at the ISR[2].

Assuming a 30 cm H_2 target, 10^7 incident π^- per pulse and a trigger solid angle of 2.2 sr, we obtain a rate of 1 event/pulse with $P_t > 3$ GeV/c, or about 12,000 events per day (with a safety factor of 0.5). Out of these there are ~ 1 $^\circ/_{oo}$ at $P_t \gtrsim 5$ GeV/c.

In Table 3 we show the number of events with $P_t > 3$ GeV/c which would be produced in running for 100 days with a negative beam and for another 100 days with a positive beam.

In the first stage we concentrate on $\pi^- p$ for which already a 30 days run will produce a valuable sample of data.

8. Pattern Recognition

Attention has been paid to the problem of pattern recognition. Fig. 11 shows two examples of 8-prong events[*] and gives an idea of the pattern recognition problem. The method will be to look first for tracks in the lever arm. These are in a field free region, are straight and therefore easily recognised with a minimum of ambiguities. Generation of two types of interaction, peripheral and central shows that on the average 60% of all tracks go into the lever arm where they will be easily recognised. Tracing these

tracks back into the vertex detector will enable the points belonging to them to be removed. We are then left with the wider angle tracks of < 10 GeV/c to recognise in the vertex detector. This we have studied with the proposed arrangement. The fact that we have accurate (xyz) points in space allows the pattern recognition to be done in space rather than in projection and helps to remove ambiguities. Two methods are available: the first called the principal component method deals well with 5 and 6 points tracks and, after these are removed the second method or "spline fit" deals with the remaining tracks having 3 or 4 points.

In order to avoid a superposition of events we inhibit the wire chamber system during one memory time after each interaction in the target.

9. Data Acquisition

The data acquisition will be done on a PDP11 computer supplied by CAEN University; the system is capable of recording 100 events/burst. Since the predicted trigger rate for $P_t > 3$ GeV/c is $\sim$ 20 events/burst (par. 6) we have a considerable margin in hand. For running in the spectrometer it would help to have in parallel an independent more powerful control computer, for instance, the IBM 360/44 already existing in the NP Division. This may be used at a later stage for data reduction such as selection of events with at least one high P_t particle, so reducing the number of tapes and the load on the central computer.

10. Cost Estimate

We have estimated the cost as follows:

Vertex detector (16 000 wires)	1.35	MSF
Lever arm - drift chambers	0.75	
MWPC in beam region	0.14	
4 Cerenkov counters	1.10	
Hodoscope trigger system	0.40	
Data acquisition equipment	0.30	
	4.04	MSF
MAGNET (17 kg 2m Ø x 1.2 m)	1.50	
TOTAL:	5.54	MSF

III. MOTIVATIONS

The start up of the ISR and the NAL machines have given us tools for probing the structure of the nucleon in finer detail than possible before. First experiments on these machines have yielded several interesting results some of which are:

(a) the p-p total cross section increases by about 10% in the energy range 50-1500 GeV [1];

(b) a marked dip exists in the pp elastic differential cross section at $t = 1.5$ GeV^2 [1];

(c) many more particles are found at high P_t (fig. 12) ($P_t > 1$ GeV/c) than are predicted from a simple extrapolation of the well known distribution ($\alpha\ e^{-6P_t}$) at low P_t [2,3,4,5,6].

(d) the particle composition of high P_t events depends on P_t [2,5].

Much theoretical speculation exists in the literature on the underlying causes of these observations, not the least interesting of which is the interpretation of all these data in terms of the collisions of point like objects (e.g. partons, quarks) contained inside the proton [7]. The question arises as to whether we are seeing a similar effect as was observed in the classic Rutherford scattering experiments, where the excess of particles with a large momentum transfer over that expected from purely Coulomb effects was attributed to a point like nucleus contained inside the atom.

It is clearly of interest to investigate the above phenomena in order to see if indeed we are beginning to see a structure inside the proton. It is thus the purpose of the present proposal to explore, in more detail the characteristics of the interactions in which a high P_t particle emerges, carrying as it does, information on the structure of the proton down to distances of $h/P_t = 4 \times 10^{-15}$ cm. It is clear that such an experiment makes sense, if only to see whether such a special class of interactions has a different behaviour from the peripheral ones.

An apparatus to study, in reasonable detail (almost complete particle momentum and angle determination along with particle identification over a large c.m.s. solid angle) is not constructed in one week and it is our aim to build a good piece of equipment which will be ready at SPS start up and at the same time be competitive with anything of a similar nature which might exist at NAL at that time.

One can ask if (a) such an experiment is valid at the SPS as compared to the ISR, and (b) should one not wait a further period and do the experiment in the North area at 300 GeV/c. We discuss points (a) and (b) in more detail.

Point (a): SPS versus ISR. The $d\sigma/dP_t$ variation as a function of P_t and $\sqrt{s}$ has been established to be well represented around 90° in c.m. by the expression

$$\frac{d^2\sigma}{d\Omega\, dP_t} \propto \frac{1}{P_t^{7.24}} e^{-26.1\, P_t/\sqrt{s}} \qquad (4)$$

If we compare the SPS at 150 GeV/c ($\sqrt{s}$ = 16.8 GeV) with the ISR at $\sqrt{s}$ = 52 GeV (26 GeV + 26 GeV) we find that for equal instantaneous interaction rates the $d\sigma/dP_t$ are equal when P_t = 5 GeV/c (x_t = 0.6) at the SPS and P_t = 8 GeV/c (x_t = 0.3) at the ISR. We may compare these values in various ways:

(i) if a particle with transverse momentum is thought of as carrying with it information from a region characterised by a dimension of $x = \hbar/P_t$ (4×10^{-15} cm at 5 GeV/c) then we can compare this to the dimension we can study at the ISR (2.5×10^{-15} cm);

(ii) if we are trying to observe jets then the $\gamma\beta$ transformation factor of a jet of mass M is P_t/M. The change in the $\gamma\beta$ factor of 1.6 in going from a P_t = 5 GeV/c to a P_t = 8 GeV/c, although useful, is unlikely to be the reason which would make jets observable. In that respect, it is more important to be able to identify the

particles which could constitute a jet opposite to the high P_t particle, since the Lorentz transformation from laboratory to c.m.s. is mass-dependent for small c.m.s. momenta (see fig.13). This implies particle identification over a large c.m.s. solid angle. This can be achieved at the SPS.

(iii) an increase in the multiplicity of the particles produced opposite to a high P_t π^o has been observed at the ISR as P_t is increased. However, this increase must come down at $x_t = 2P_t/\sqrt{s} = 1$ as we are then dealing with pp elastic scattering. At the SPS we can study high x_t and this may turn out to be of interest;

(iv) the availability, at the SPS, of other kinds of incident particles (π, K, $\bar{p}$) make it possible to search for characteristics dependent on the incident particle makeup ($q\bar{q}$ for π, qqq for proton for example).

The conclusions are summarised in Table 4.

Point (b): West Area versus North Area. In order to understand the nature of the high P_t interactions it may well be necessary to study them at various incident energies. The variation of $d\sigma/dP_t$ with incident energies 75, 150, 200 and 300 GeV/c is shown in fig. 14. For 150 GeV/c we see that at P_t = 3 GeV/c the signal above the extrapolated e^{-6P_t} curve is a factor 10. At 75 GeV/c this factor is only 2 and one needs to go to a P_t = 40 GeV/c to recuperate the factor 10 with an associated drop in rate by a factor 100. At 150 GeV/c we expect 12000 ev./day with P_t > 3 GeV/c. Clearly the rates at 300 GeV/c are greater (between 2 and 5*)). We believe, since the "high P_t effect" exists at 150 GeV/c and the rates above P_t = 3 GeV/c are adequate that one should not wait two years before undertaking such studies.

As an example of the present interest in studying high P_t reactions at energies less than 300 GeV/c we point out the marked difference in the p/π^+ ratio between 200 and 300 GeV/c, as shown in fig. 15. The reason for this marked variation is not understood.

*) We read a factor of 2 from the British-Scandinavian-ISR data (Ref. 2) extrapolated to our $\sqrt{s}$. We calculate a ratio of 5 from the CERN-Columbia-Rockefeller data (Ref. 4).

Finally, in order to demonstrate the interest of the proposed experiment we list some of the questions which it could help to answer.

(a) Do jets occur? i.e. are there several closely correlated particles in the P_t, P_L plot, as shown in fig. 13, which might be suggestive of local parton-parton type scatterings?

(b) What is the multiplicity and particle composition in a jet?

(c) What is the mass distribution of the jets?

(d) How often is a high P_t particle on one side associated to a high P_t particle of the other side?

(e) How do the properties of the interactions depend on whether the high P_t particle is a π, K, p or $\bar{p}$?

(f) Are quantum numbers locally conserved; e.g. is a high P_t proton balanced by an antiproton in the opposing jet? [8].

(g) Are there observable differences between incident pions ($q\bar{q}$) and protons (qqq) as illustrated in fig. 16?

(h) What happens to the projectiles after the collision? Do they remain as peripheral fragments?

(i) How do high P_t effects at SPS energies differ from those at ISR energies?

(j) Are there any new high mass objects, e.g. do massive fireballs, charmed particles etc. exist?

(k) What is the percentage of events with no neutral particles? Can we obtain a completely analysable sample of 4 constraint fit events?

Although undoubtedly some of these questions will be answered others will probably appear.

REFERENCES

1. e.g. U. Amaldi, Rapporteur's talk, Aix-en-Provence, 1973.

2. M. Banner et al., Phys. Letters 44B (1973) 537.

3. B. Alper et al., Phys. Letters 47B (1973) 75 and 275.

4. F. W. Busser et al., Phys. Letters 46B (1973) 471.

5. J.M. Cronin et al., Phys. Rev. Letters 31 (1973) 1426.

6. D.C. Carey et al., NAL-Pub 73/72-EXP 7100.063. Submitted to Phys. Rev. Letters.

7. J.O. Bjorken: "Can we measure parton-parton cross sections?" SLAC-PUB-1280 (1973) and further theoretical references therein.

8. E.L. Berger and D. Branson, Phys. Letters 45B (1973) 57.

TABLE 1: Particle fluxes in the H1 beam W.A. at 150 GeV/c (per 10^{12} protons at 200 GeV/c, $\Delta\Omega$ = 10μsterad, and $\Delta p/p = \pm 0.5\%$).

negative beam		positive beam	
particle	number/pulse	particle	number/pulse
π^-	6.6×10^6	π^+	2.7×10^7
K^-	2.6×10^4	K^+	5.6×10^6
$\bar{p}$	3.0×10^3	p	2.5×10^9

TABLE 2: Čerenkov Counters *)

Counter	gas filling at atmospheric pressure	length L(m)	N_{O-1} (cm^{-1})	P_{min}	P_{max}	P_{min}	P_{max}	P_{min}	P_{max}
Č1	n-penthane gas	0.5	100	2.5	10.1	9.0	19.0	2.5	19.3
Č2	CO_2	1.1	160	5.2	20.3	18.3	37.7	5.2	39.0
Č3	H_2	1.8	160	10.7	32.3	37.7	60.4	10.7	61.8
Č4	Ne	3.0	160	17.0	44.4	60.4	83.7	17.0	84.6
				π-K separ.		K-p separ.		π-p separ.	

*) The limits quoted are for a Čerenkov efficiency of 95%.

TABLE 3: Expected number of events with $P_t > 3$ GeV/c *) for 100 days each in a negative and a positive beam

negative beam	Events	positive beam	Events
π^-	10^6	π^+	11000
K^-	4000	K^+	2000
$\bar{p}$	500	p	10^6

TABLE 4: Comparison of SPS vs ISR for high P_t studies

Quantity	ISR	SPS	Comments
P_t^{max} at equal rate **)	8 GeV/c(X_t=0.3)	5 GeV/c(X_t=0.6)	
"probing the proton": resolution $\Delta X=\hbar/p_t^{max}$	2.5 x 10^{-15} cm	4.0 x 10^{-15} cm	ISR has some advantages
"jet focusing" in c.m. $\gamma_{jet} = P_t/M_{jet}$	ratio 1.6 : 1		
particle identification	difficult due to low momenta and large lab solid angle	easy due to Lorentz transformation (use of standard gas C counters)	SPS better
variation of incident projectile	not possible	easy for πp,pp possible for Kp	SPS experiments necessary
threshold effects in P_t (e.g. p/π^+ ratio)	not so easy	$p_{inc} \gtrsim 50$ GeV/c available	SPS experiments necessary

*) assuming equal high P_t cross sections for the different incident particles.

**) $\sim$ 10 per day; we recall that the ISR luminosity corresponds to $\sim 10^7$ particles on a 30 cm H target

FIGURE CAPTIONS

Fig. 1a Plan view of the apparatus.

Fig. 1b Elevation view of the apparatus.

Fig. 2a Momentum resolution $\Delta P/P$ versus the lab. momentum P for particles inside the vertex detector as a function of transverse momentum.

Fig. 2b Mass resolution M/M versus momentum of the particle of mass $M(P_M)$ where M decays into $\pi^+\pi^-$ in the vertex detector.

Fig. 3 Kinematic curve in the c.m.s. for the reaction $\pi^- p \to \pi^- X$ at 150 GeV/c. P_t is plotted against $X_{11} = 2P \cos\theta^*/\sqrt{s}$. Curves of constant lab. angle and constant P_{lab} are shown as is the region of acceptance of the trigger system. The heavy lines show the limits for different particle identification.

Fig. 4 Resolution in the transverse momentum $\Delta P_t/P_t$ versus P_t for particles traversing the lever arm system.

Fig. 5 Ranges in momentum for πp, Kp, πp identification in the different Čerenkov counters.

Fig. 6 View of the Čerenkov mirror system as seen by viewing along the beam. The 10 mirrors above the beam reflect light into 10 photomultipliers, as shown in the plan view. The same is true for the 10 mirrors below the beam. The 8 shaded mirrors (4 above, 4 below beam) reflect light from the triggering particle into 4 + 4 separate photomultipliers. The histogram shows, for eight prong events, the probability of a given mirror having a particle incident on it. On average there is a three mirror separation between particles.

Fig. 7 Side view of the Čerenkov mirror system showing the separate mirror for triggering on the high P_t particles (shaded region).

Fig. 8 Arrangement of the ring of hodoscoping counters at 3.5 m from the target, as viewed from along the beam. Each element is 1 cm wide.

Fig. 9a Disposition of co-ordinate system in a plane perpendicular to the field direction for the counter hodoscopes M_1 and M_2. ℓ = distance of target to mid point of magnetic field.

Fig. 9b Example of the correlation y_1 vs y_2 in the horizontal plane for different particle momenta and c.m.s. emission angle.

Fig. 10 Results from generating a uniform distribution of tracks in X_t (= $2P_t/\sqrt{s}$) and X_{11} in the c.m.s. and tracing them into the trigger system consisting of two ring shaped hodoscopes M_1 and M_2.

(a) y_1 vs y_2 correlation for tracks with $80^\circ < \theta^* < 100^\circ$ and $P_t >$ 3 GeV/c;

(b) longitudinal lab momentum selection from tracks of all P_t and θ^*;

(c) selection on the P_t vs θ^* plot by the matrix correlation;

(d) projection of (c) on the θ^* axis;

(e) projection of (c) on the P_t axis.

Fig. 11 Appearance of two 8 prong events at 150 GeV/c in a plan view of the apparatus.

Fig. 12 Invariant cross section $E\, d^3\sigma/d^3P_t$ vs P_t for the reaction $pp \to \pi^\circ$ + anything at the ISR (Results from the C.C.R. Collaboration).

Fig. 13a Hypothetical $\pi^- p \to$ 12 particle interaction at 150 GeV/c.giving rise to one high transverse momentum particle, a jet of 7 particles and the fragments of the incident and target particles.

Fig. 13b Transformation of the same event into the lab. system.

Fig. 14 Invariant cross section $E\, d^3\sigma/d^3P_t$ vs P_t for the reaction $P + W \to \pi^-$ + anything at 200 and 300 GeV/c. (Cronin et al. at NAL). Also shown are the curves for 75 and 150 GeV/c predicted from the C.C.R. formula (see text).

Fig. 15 Variation of particle ratios as a function of X_t at 200 and 300 GeV/c (Cronin et al.).

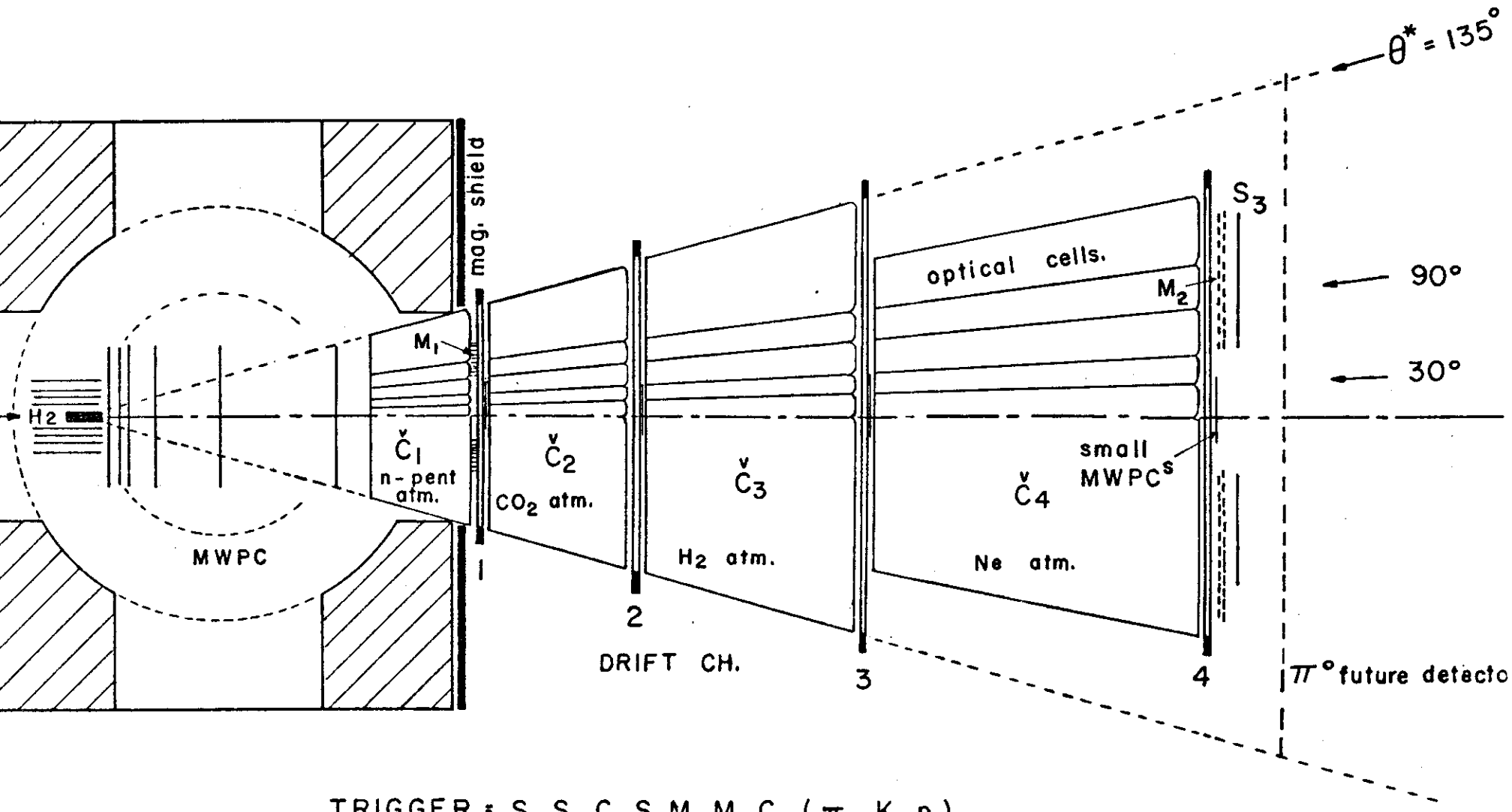

TRIGGER = $S_1 S_2 C_1 S_3 M_1 M_2 C_i$ (π , K, p)

Fig. 1a: HIGH - P_T SPECTROMETER (plan view)

SCALE ⊢ 1m. ⟶

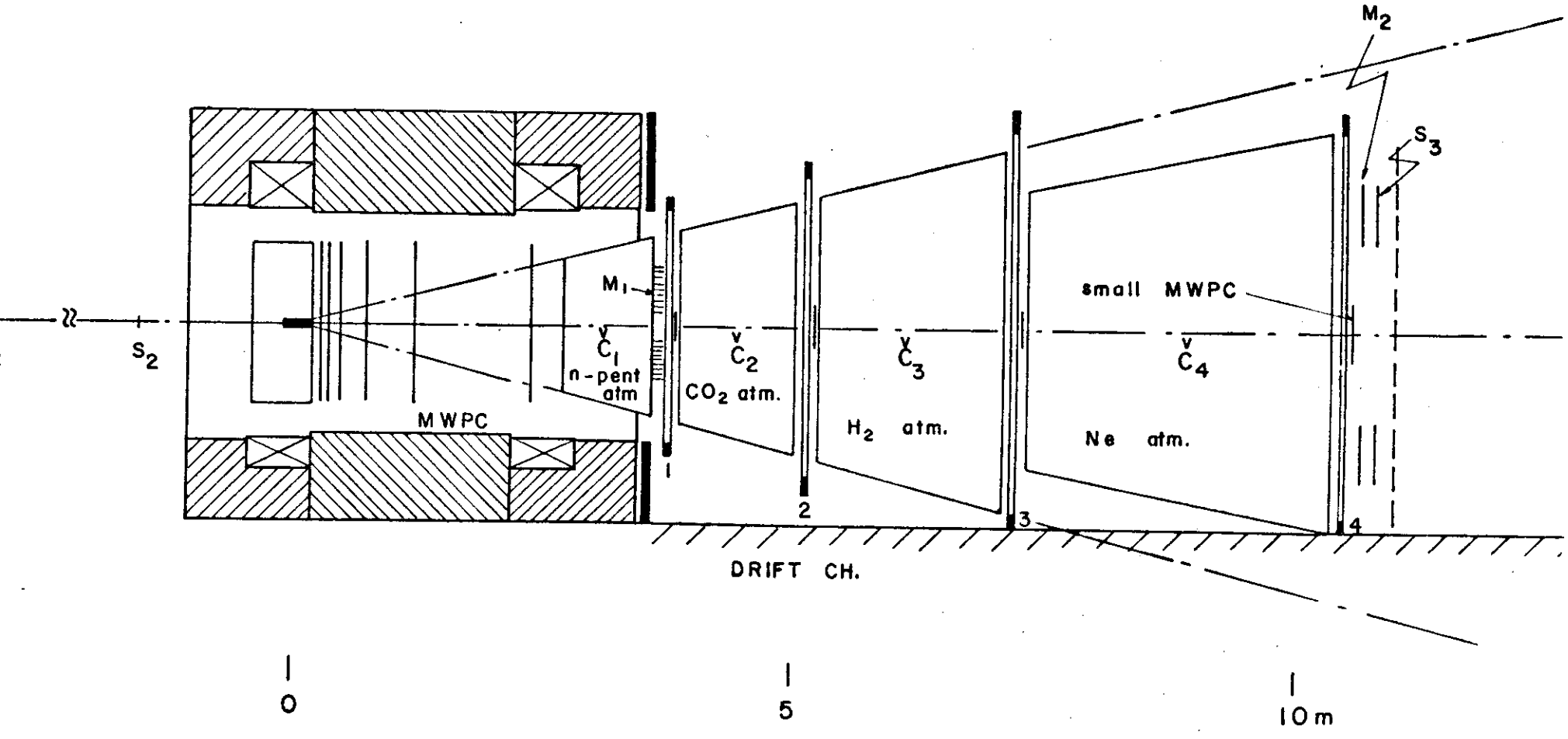

Fig. 1b : HIGH P_T SPECTROMETER (elevation)

SCALE ⟵1m⟶

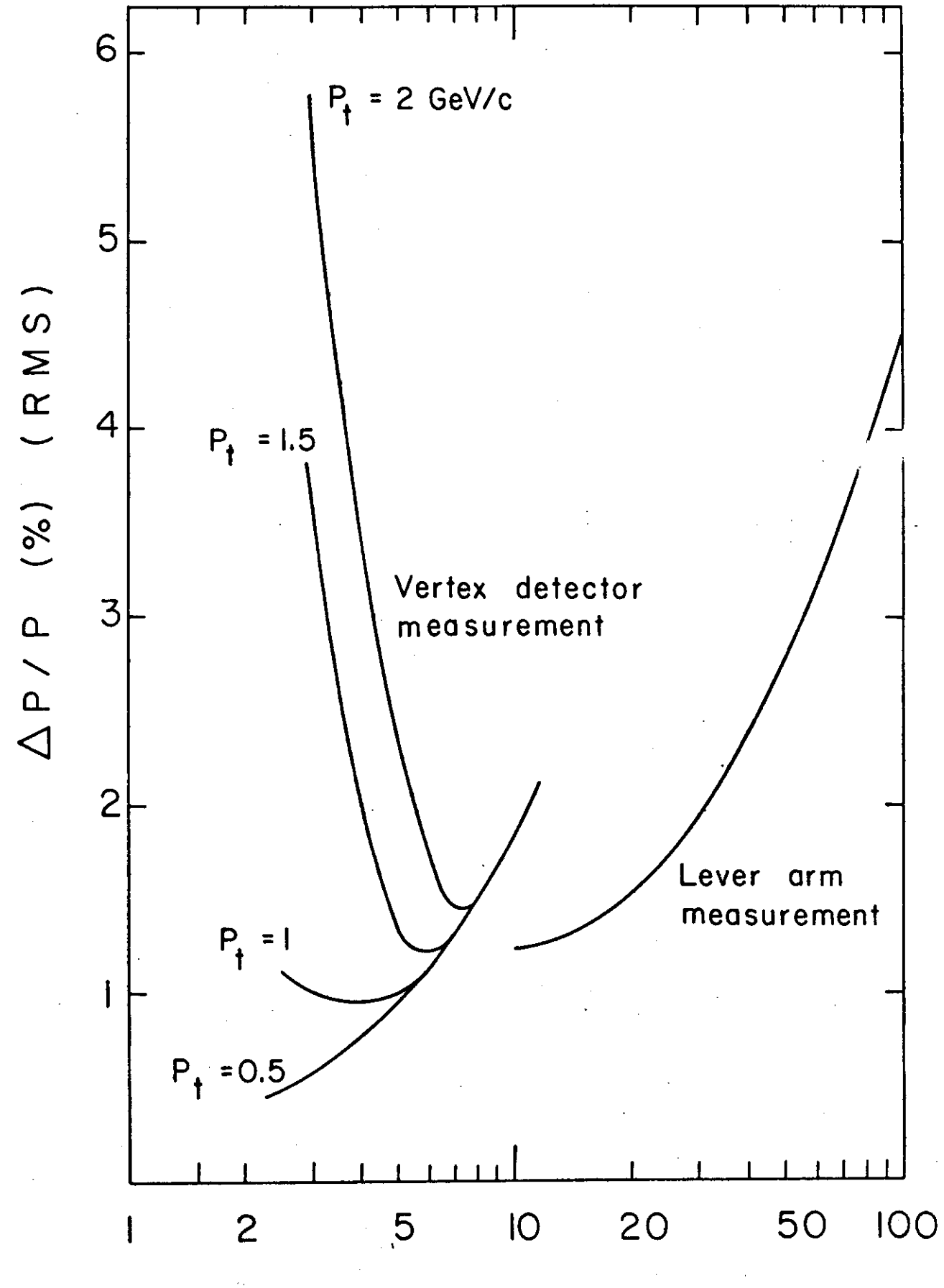
6
5
4
3
2
1
ΔP / P (%) (RMS)
P_t = 2 GeV/c
P_t = 1.5
P_t = 1
P_t = 0.5
Vertex detector measurement
Lever arm measurement
1
2
5
10
20
50
100

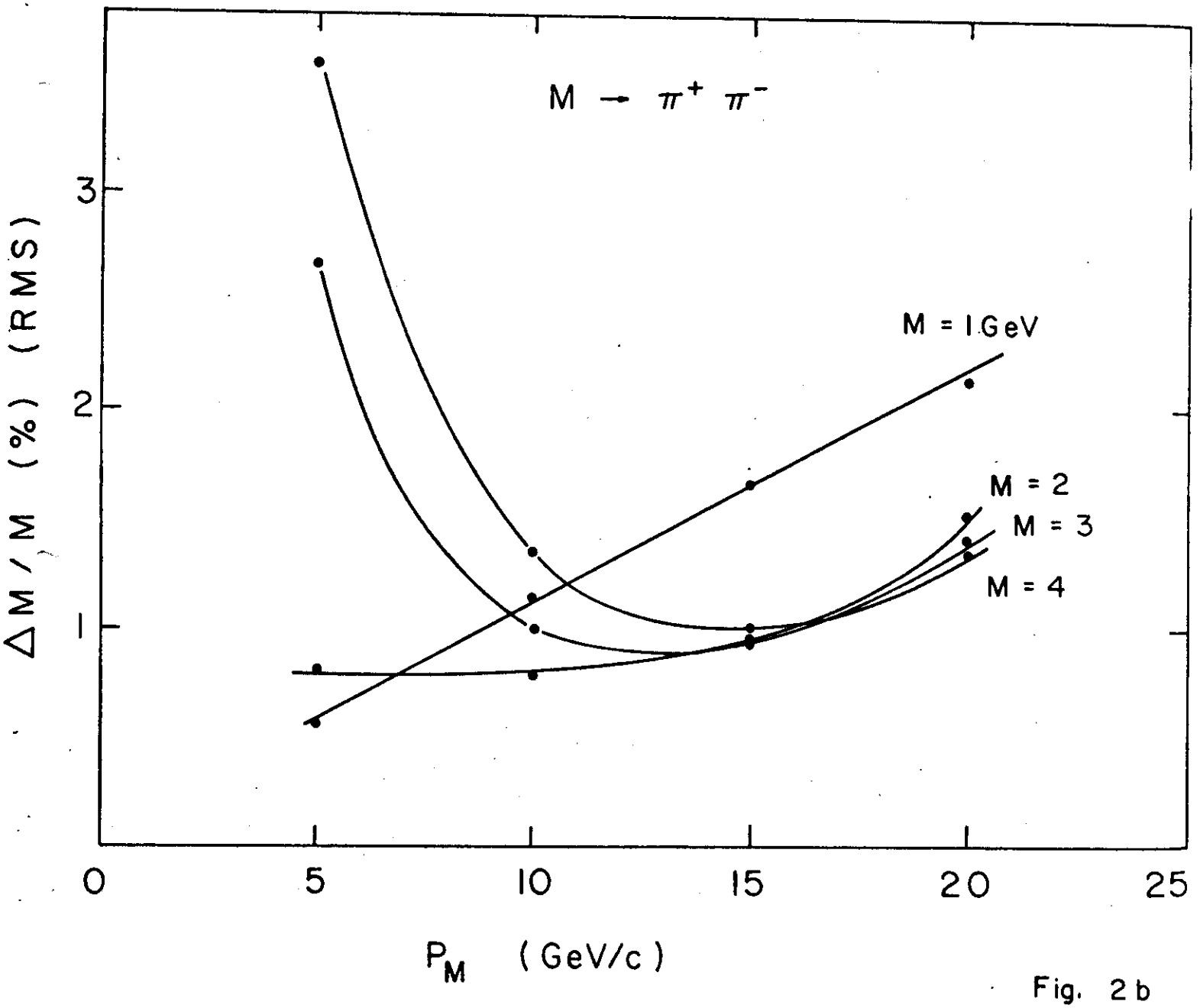

Fig. 2 b

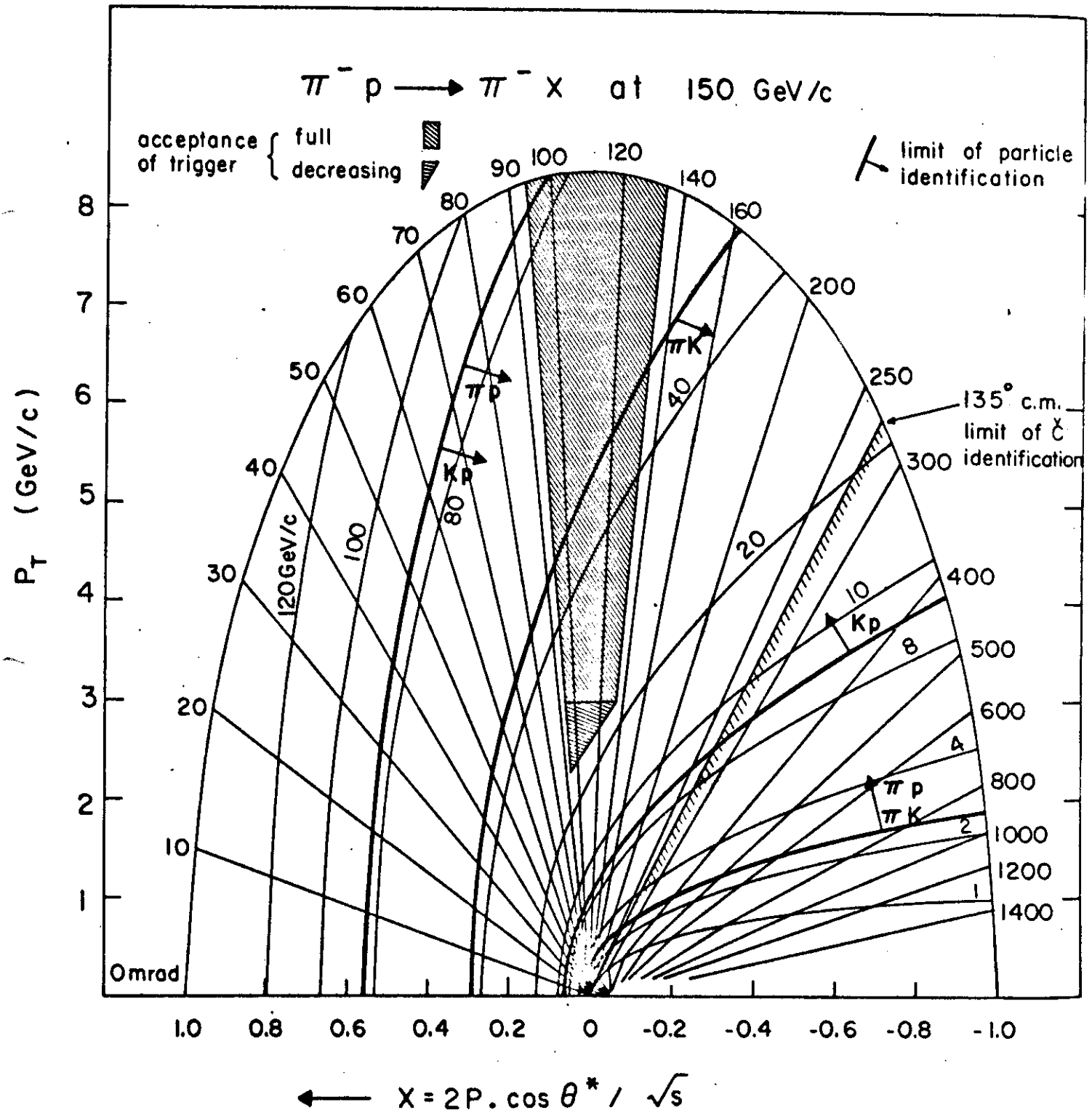
$\pi^- p \longrightarrow \pi^- X$ at 150 GeV/c
acceptance of trigger { full decreasing
limit of particle identification
135° c.m. limit of Č identification
πK
πp
Kp
πp
πK
120GeV/c
Omrad
P_T (GeV/c)
$X = 2P.\cos\theta^* / \sqrt{s}$

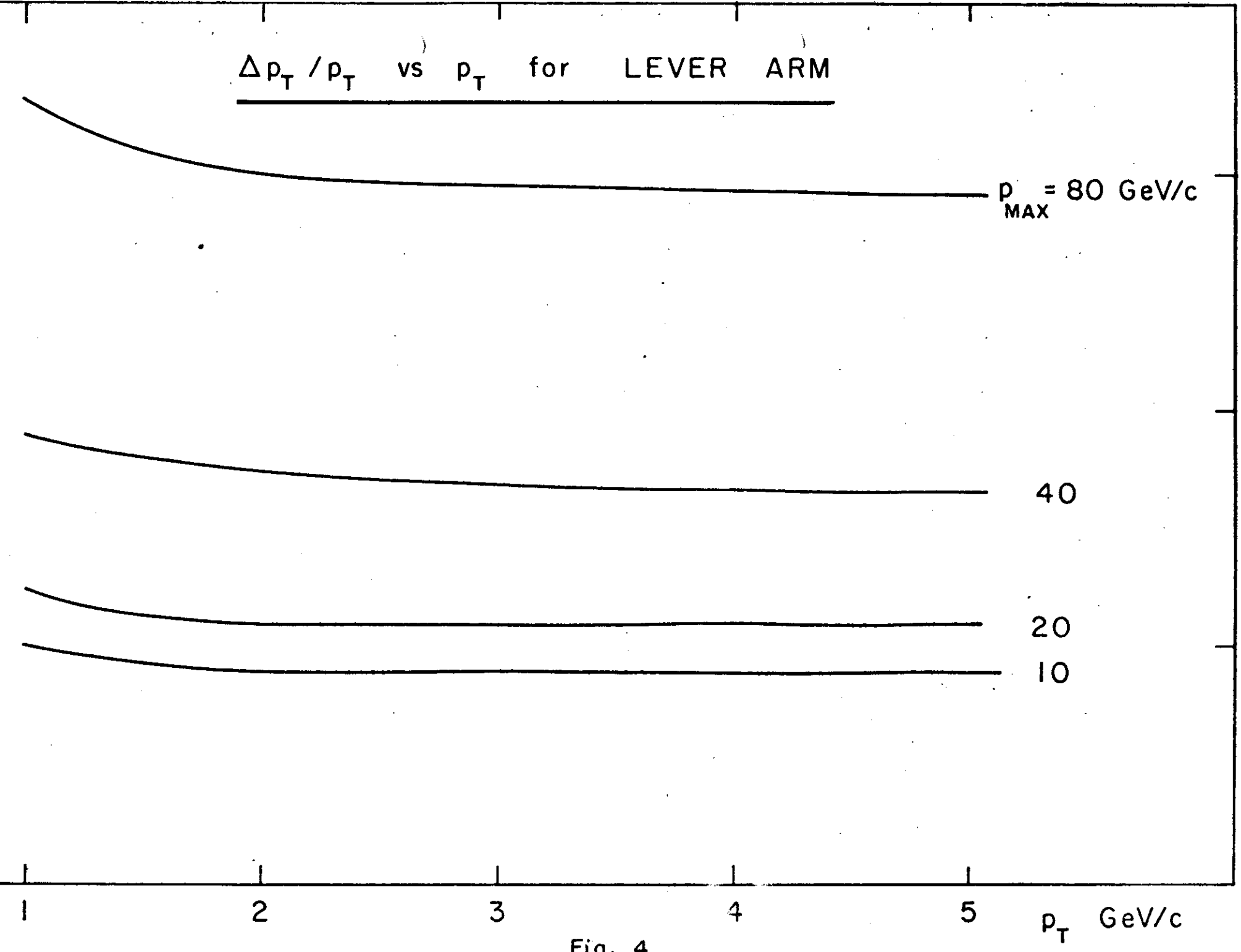
$\Delta p_T / p_T$ vs p_T for LEVER ARM
p_{MAX} = 80 GeV/c
40
20
10
1
2
3
4
5
p_T GeV/c

Fig. 4

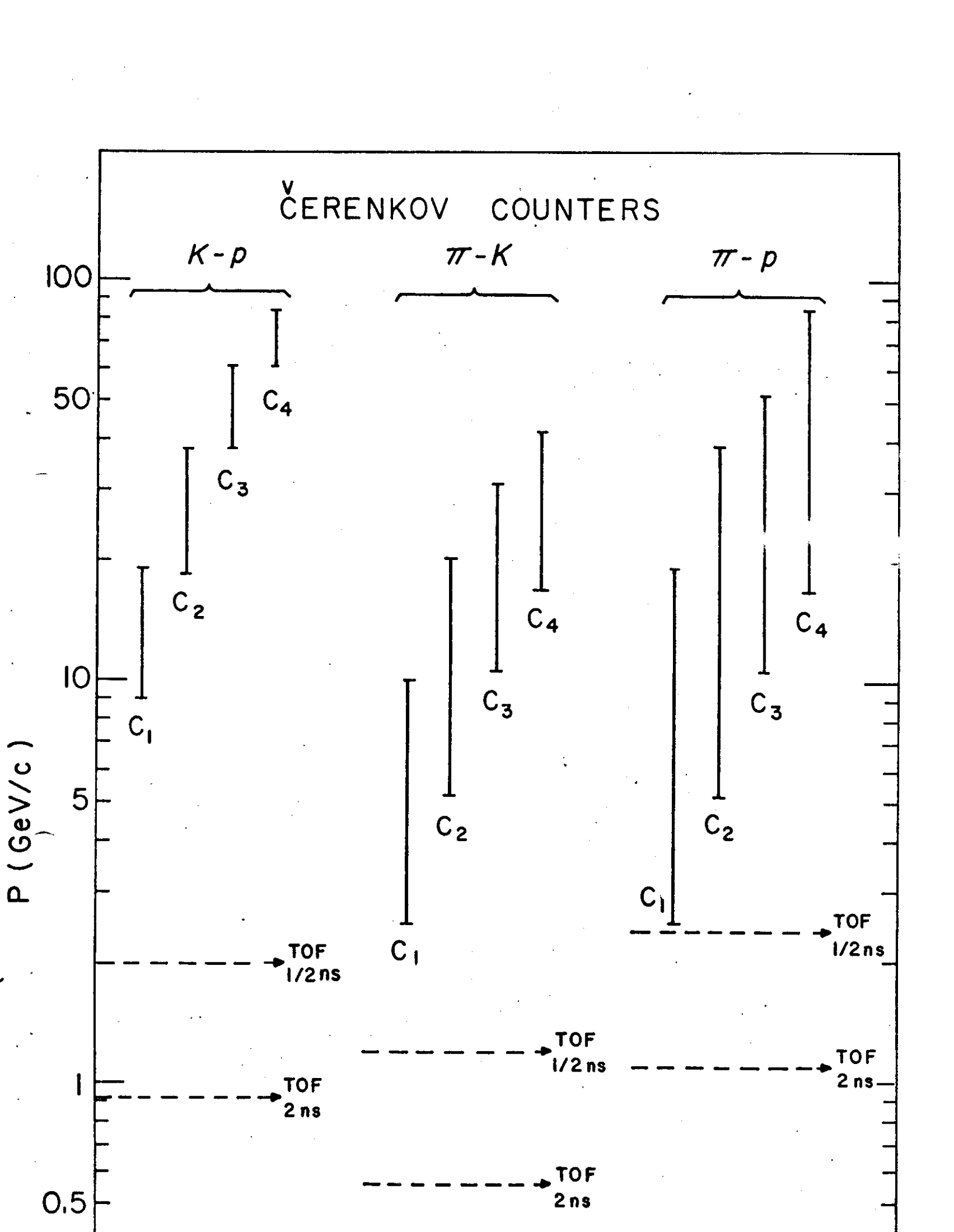
ČERENKOV COUNTERS
K - p
π - K
π - p
100
50
10
5
1
0.5
P (GeV/c)
C1
C2
C3
C4
TOF 1/2ns
TOF 2ns

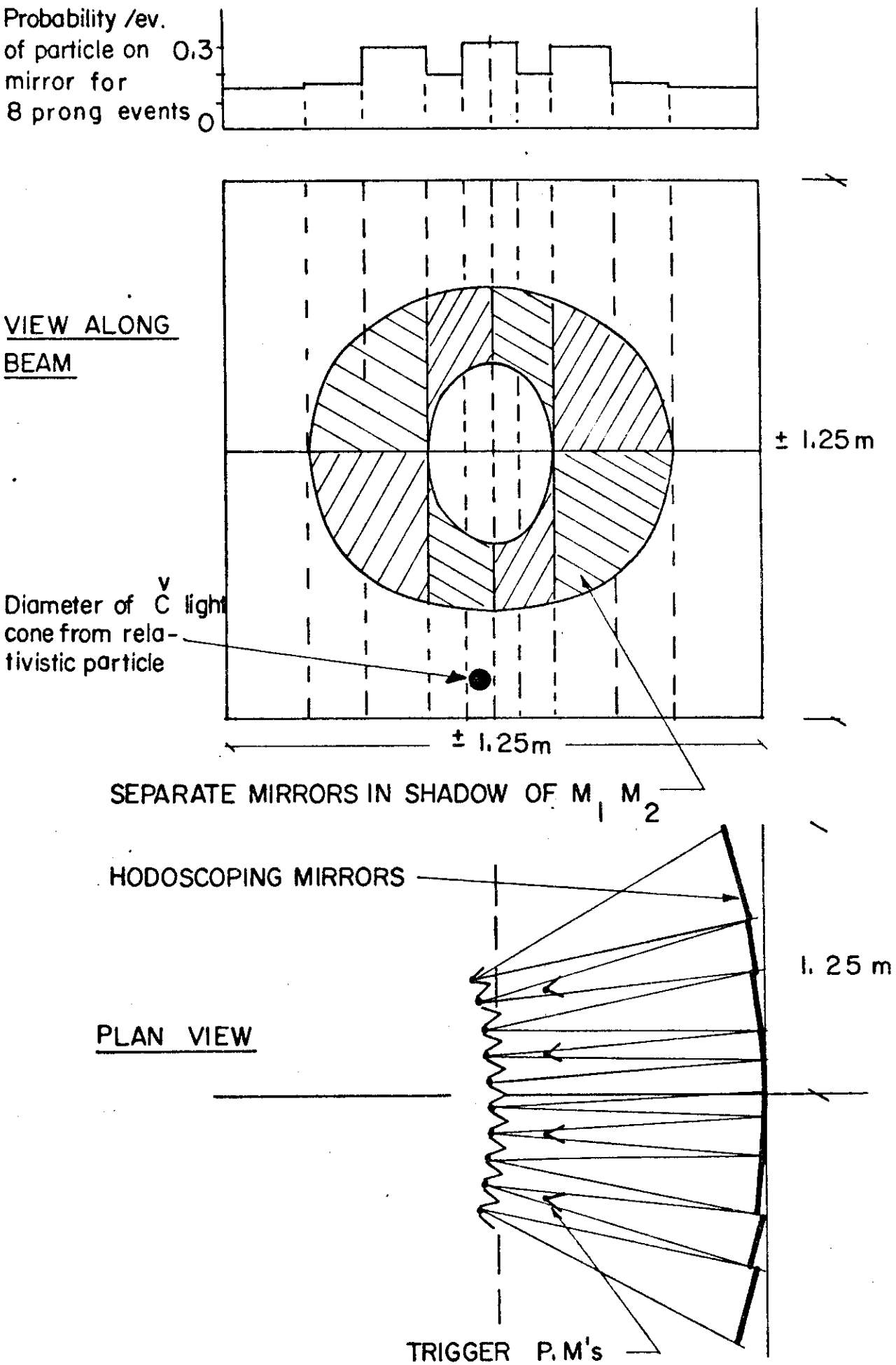
Probability /ev.
of particle on
mirror for
8 prong events
0.3
0
VIEW ALONG
BEAM
± 1.25 m
Diameter of c/v light
cone from rela-
tivistic particle
± 1.25m
SEPARATE MIRRORS IN SHADOW OF M1 M2
HODOSCOPING MIRRORS
1. 25 m
PLAN VIEW
TRIGGER P. M's

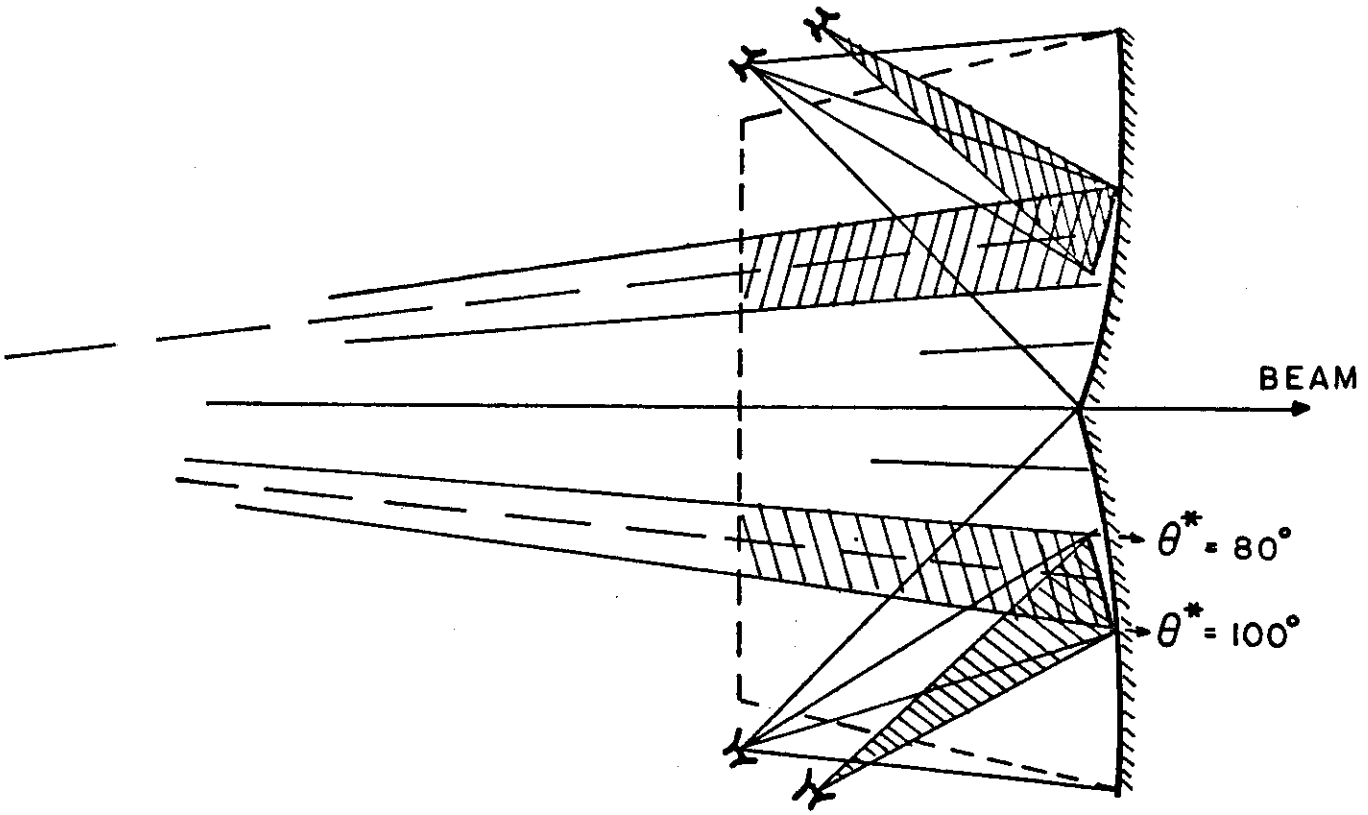

ČERENKOV MIRROR DISPOSITION (SIDE VIEW)

Fig. 7

FORMAT OF CIRCULAR HODOSCOPE AT 3.5 m. FROM TARGET

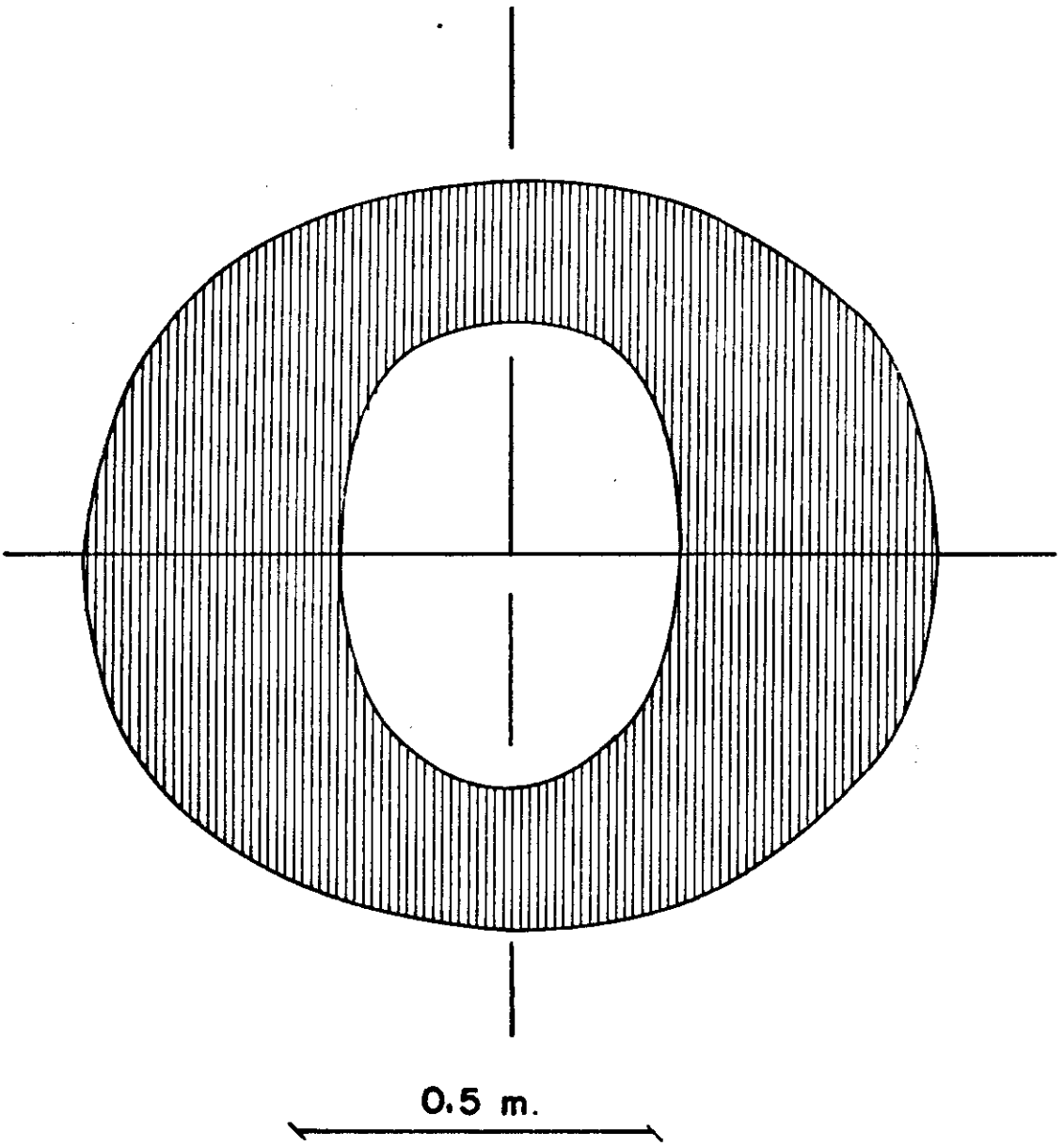

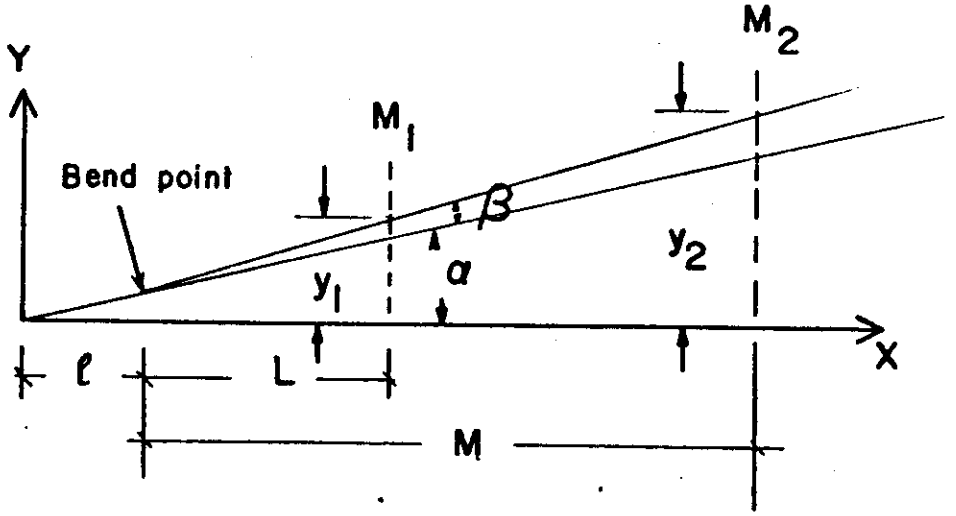

Fig. 9 a

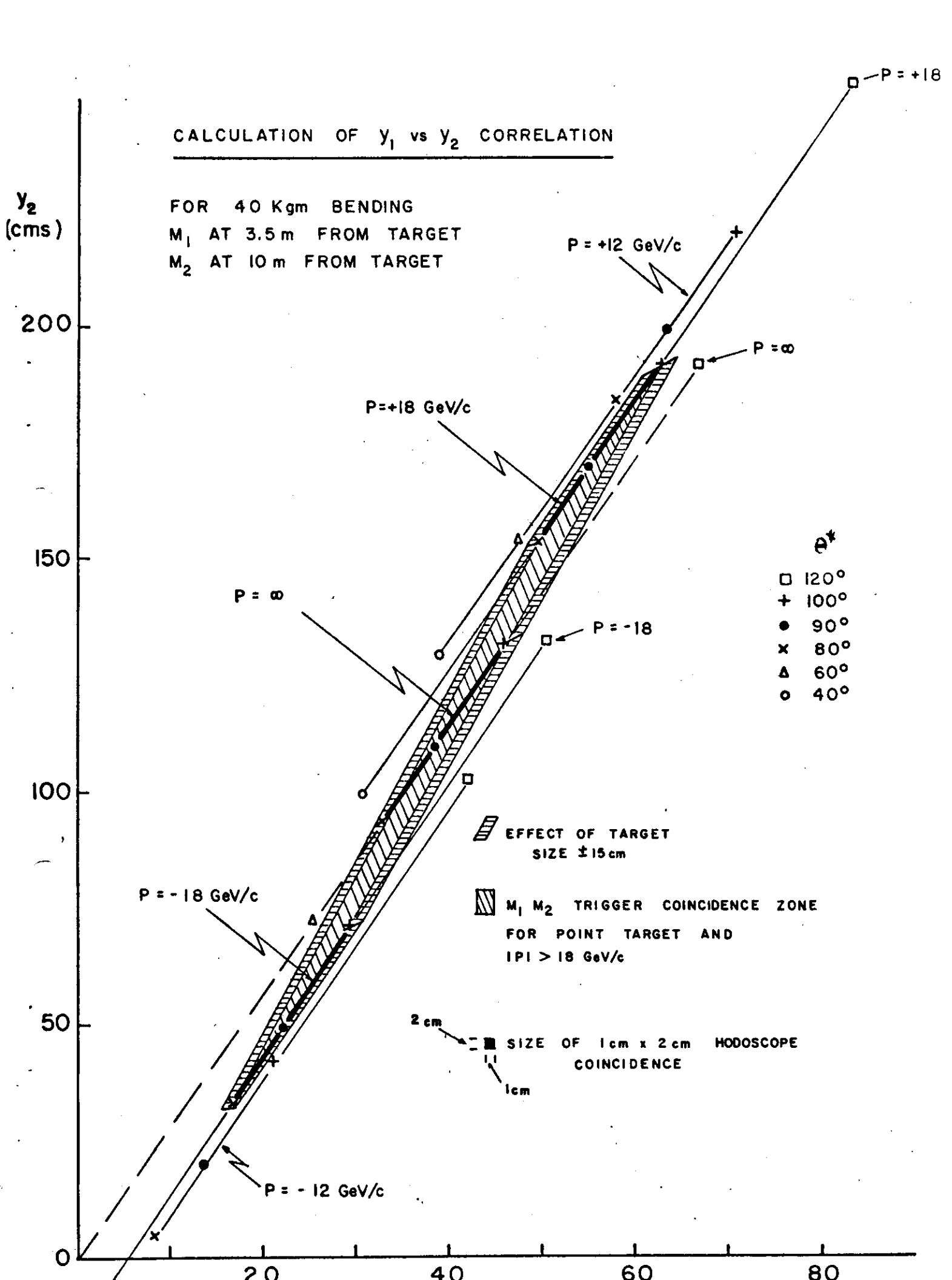
CALCULATION OF y_1 vs y_2 CORRELATION
FOR 40 Kgm BENDING
M_1 AT 3.5 m FROM TARGET
M_2 AT 10 m FROM TARGET
y_2 (cms)
200
150
100
50
0
20
40
60
80
P = +18
P = +12 GeV/c
P = ∞
P=+18 GeV/c
P = ∞
P = -18
P = - 18 GeV/c
P = - 12 GeV/c
θ*
120°
100°
90°
80°
60°
40°
EFFECT OF TARGET SIZE ±15 cm
M_1 M_2 TRIGGER COINCIDENCE ZONE FOR POINT TARGET AND IPI > 18 GeV/c
2 cm
1cm
SIZE OF 1cm x 2 cm HODOSCOPE COINCIDENCE

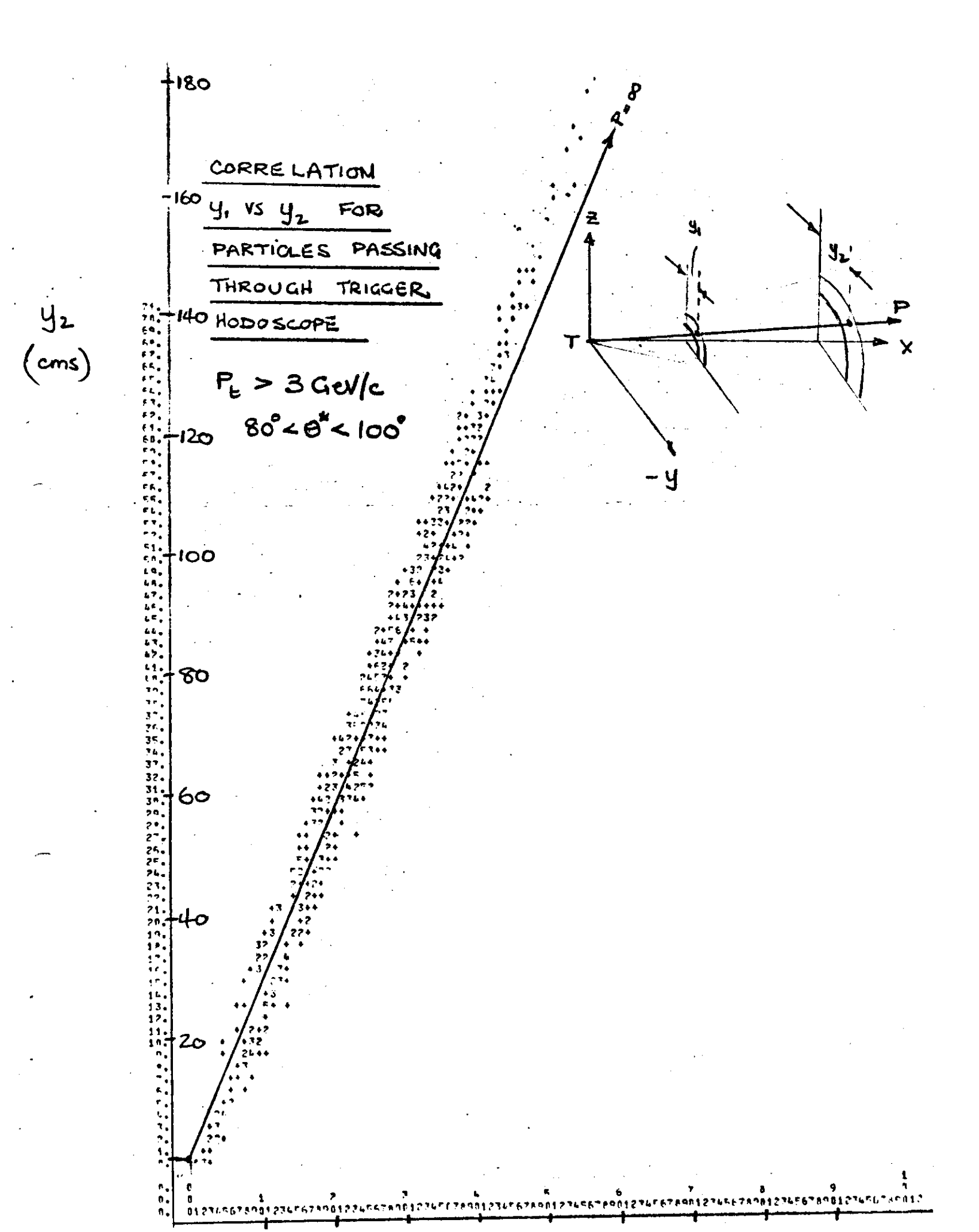
CORRELATION
y_1 VS y_2 FOR
PARTICLES PASSING
THROUGH TRIGGER
HODOSCOPE
$P_t > 3$ GeV/c
$80° < \theta^* < 100°$
y_2 (cms)
180
160
140
120
100
80
60
40
20
R=8
z
y_1
y_2
P
T
X
-y

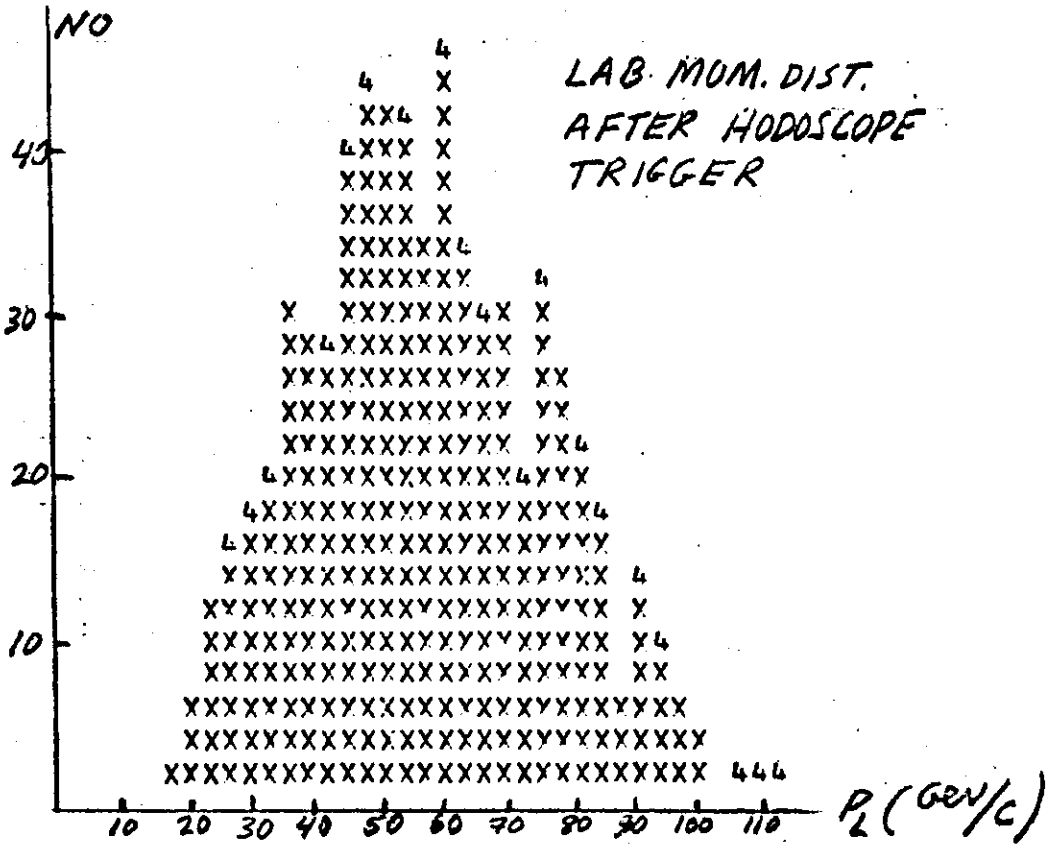
NO
LAB MOM. DIST.
AFTER HODOSCOPE
TRIGGER
40
30
20
10
10 20 30 40 50 60 70 80 90 100 110
P_L (GEV/C)

FIG. 10B.

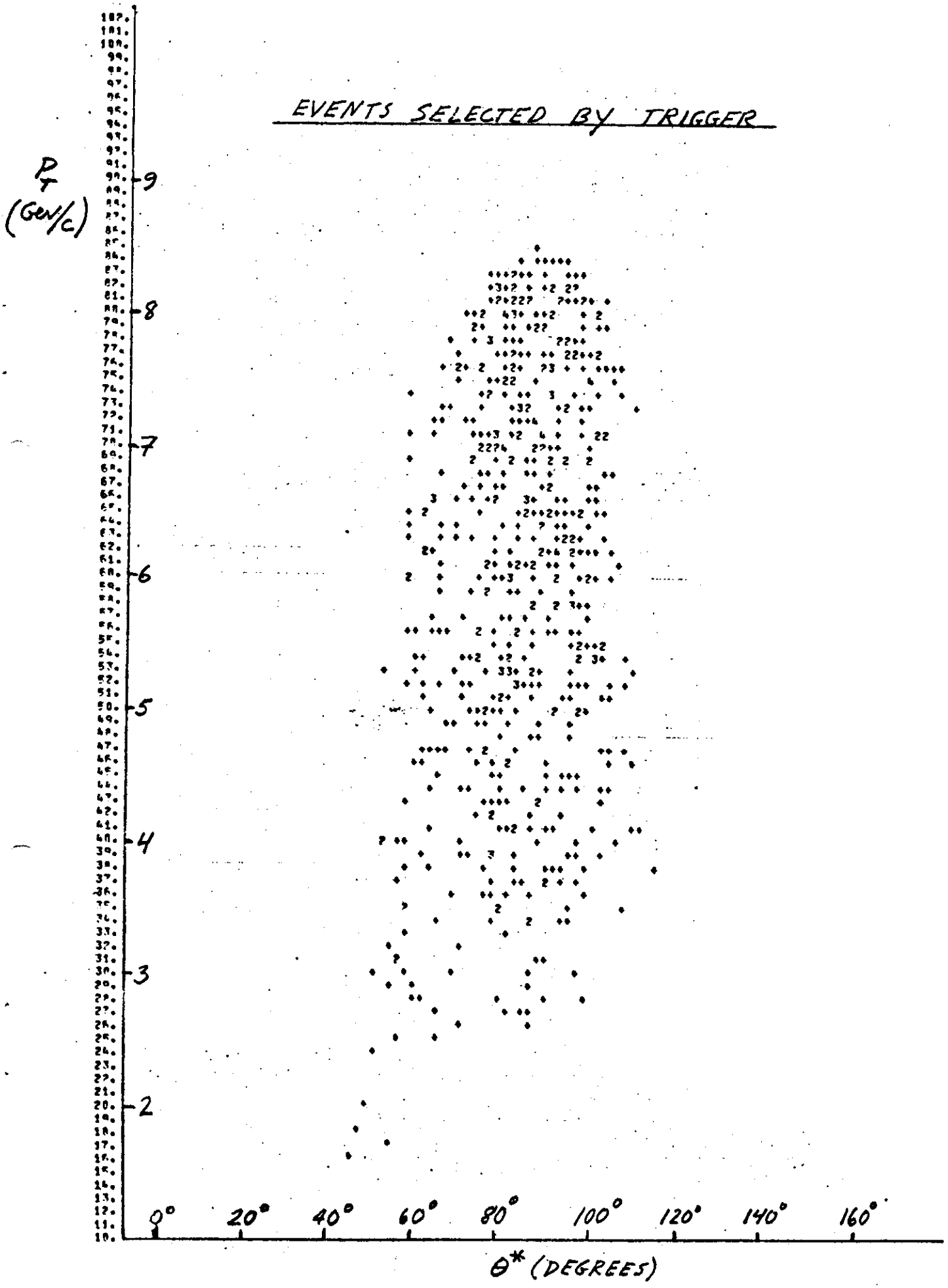
EVENTS SELECTED BY TRIGGER
P_T (GeV/c)
9
8
7
6
5
4
3
2
0°
20°
40°
60°
80°
100°
120°
140°
160°
θ* (DEGREES)

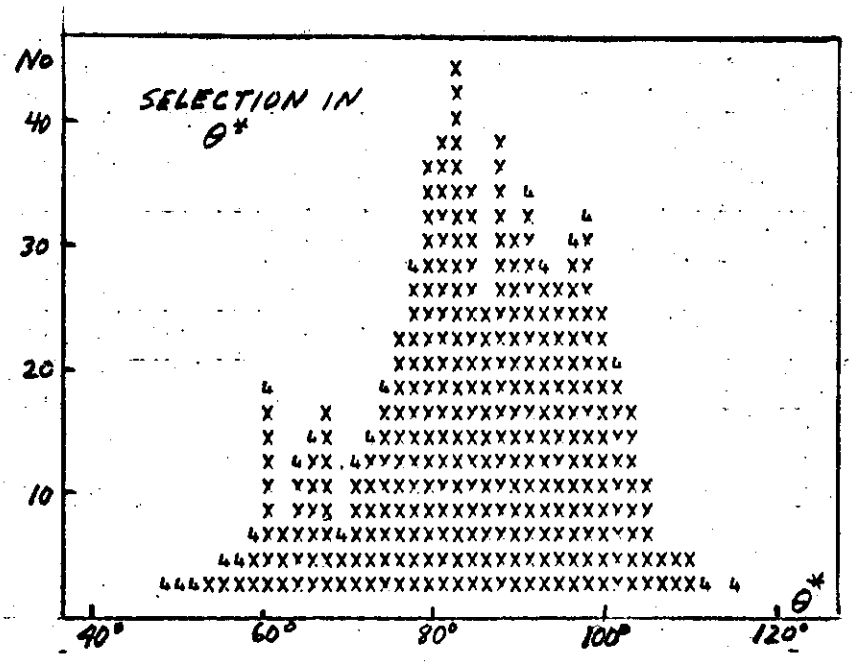

FIG 10d

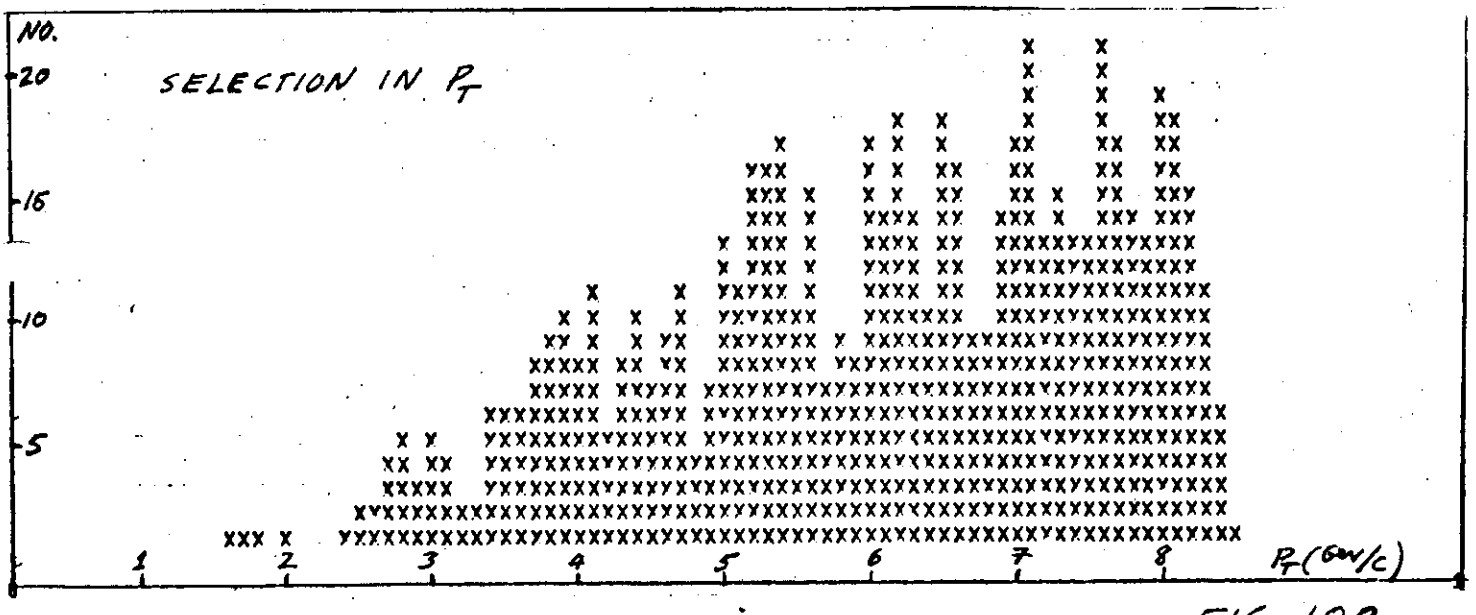

FIG. 10e

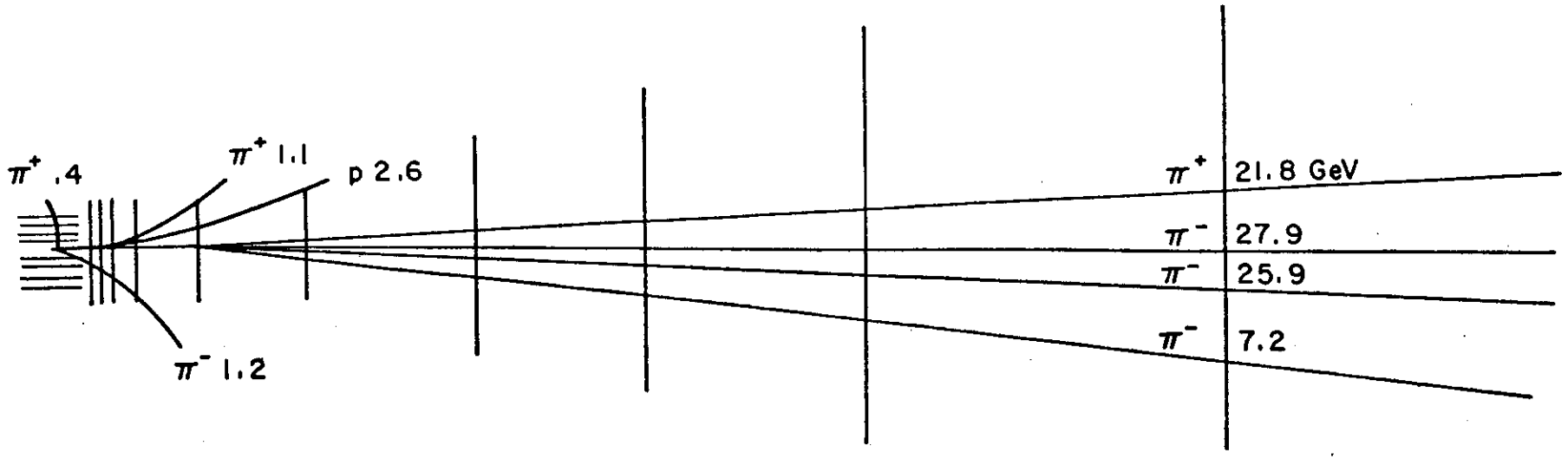

$\pi^- p \rightarrow p\, 3\pi^+ 4\pi^- \pi^\circ$ at 150 GeV/c

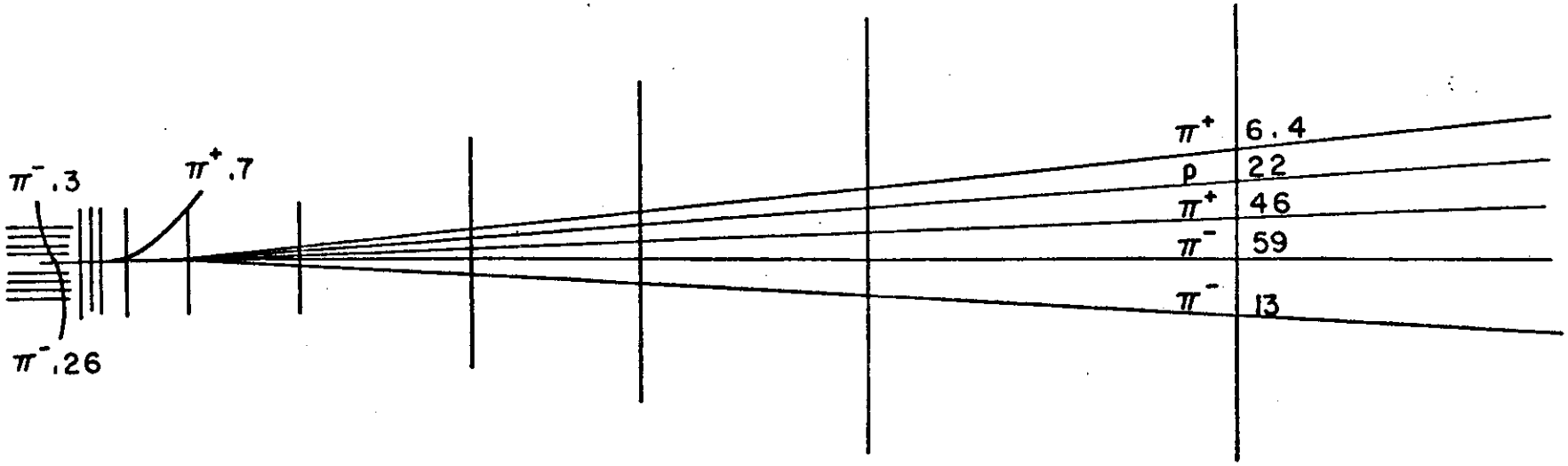

Fig. 11

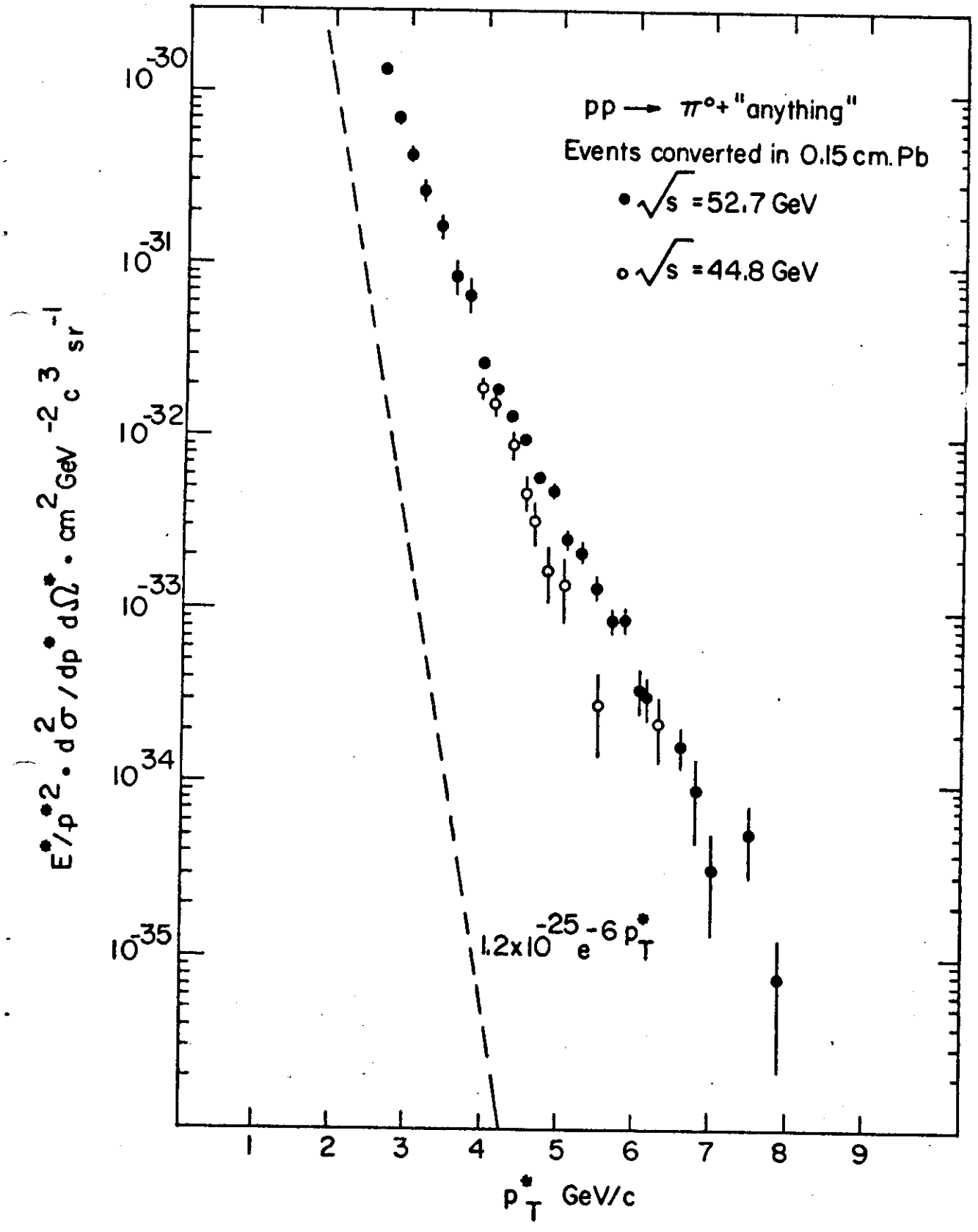
pp → π°+ "anything"
Events converted in 0.15 cm. Pb
• √s = 52.7 GeV
○ √s = 44.8 GeV
1.2x10^-25 e^-6 p*T
E*/p*2 • d2σ/dp* dΩ* • cm2 GeV-2 c3 sr-1
p*T GeV/c
10-30
10-31
10-32
10-33
10-34
10-35
1
2
3
4
5
6
7
8
9

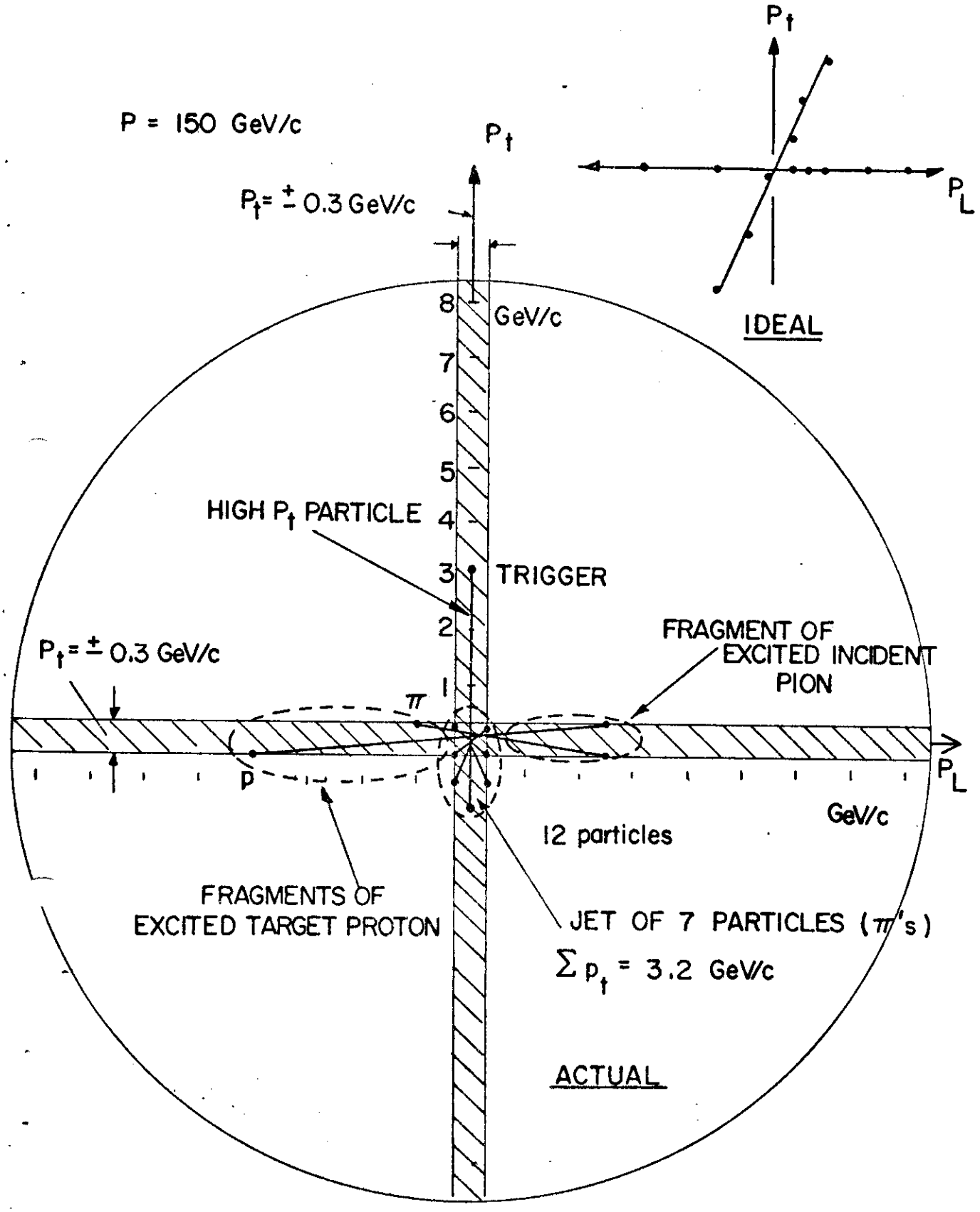
P = 150 GeV/c
P_t
$P_t = \pm 0.3$ GeV/c
8
7
6
5
4
3
2
1
GeV/c
HIGH P_t PARTICLE
TRIGGER
$P_t = \pm 0.3$ GeV/c
FRAGMENT OF EXCITED INCIDENT PION
π
p
P_L
GeV/c
12 particles
FRAGMENTS OF EXCITED TARGET PROTON
JET OF 7 PARTICLES (π's)
$\Sigma p_t = 3.2$ GeV/c
ACTUAL
P_t
P_L
IDEAL

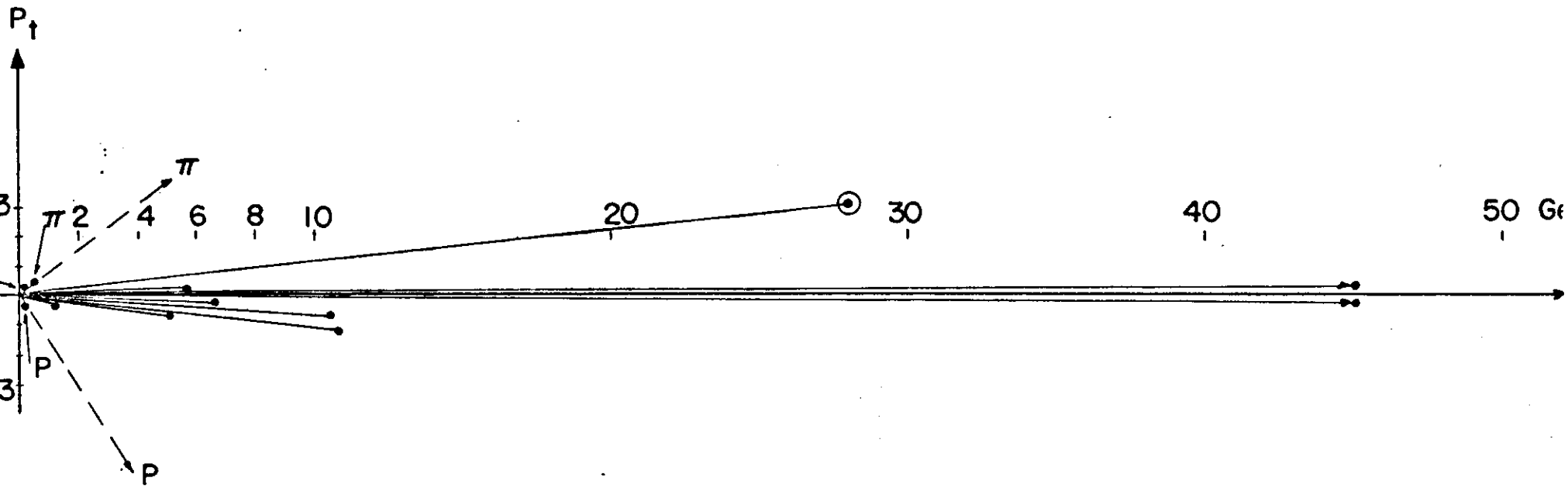

LAB. SYSTEM

E = 150 GeV/c

$\gamma_c = 9$

Fig. 13 b

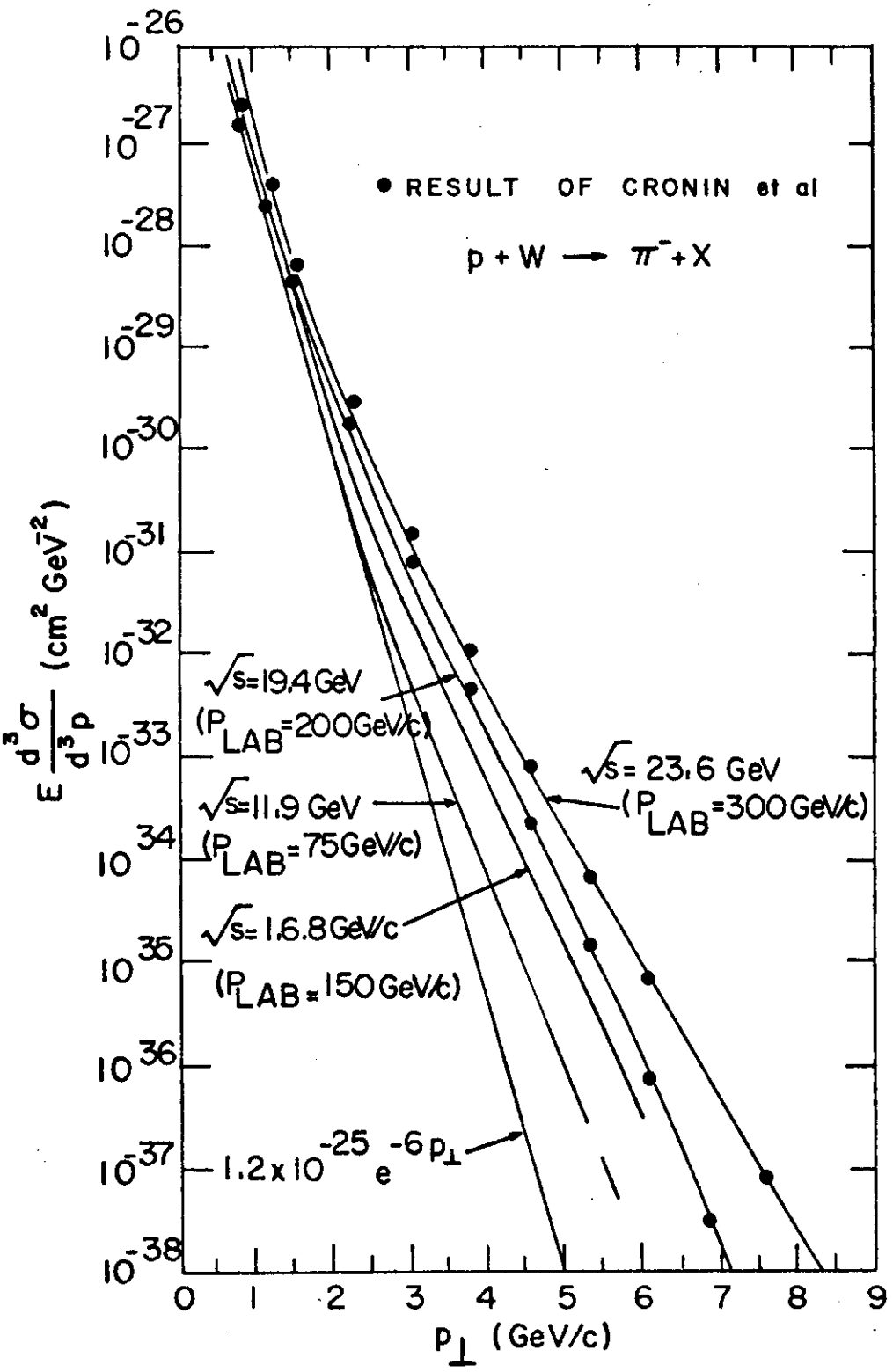
RESULT OF CRONIN et al
p + W → π⁻ + X
√s = 19.4 GeV
(P_LAB = 200 GeV/c)
√s = 11.9 GeV
(P_LAB = 75 GeV/c)
√s = 16.8 GeV/c
(P_LAB = 150 GeV/c)
√s = 23.6 GeV
(P_LAB = 300 GeV/c)
1.2 x 10^-25 e^-6 p⊥
E d³σ/d³p (cm² GeV⁻²)
p⊥ (GeV/c)

Fig. 14

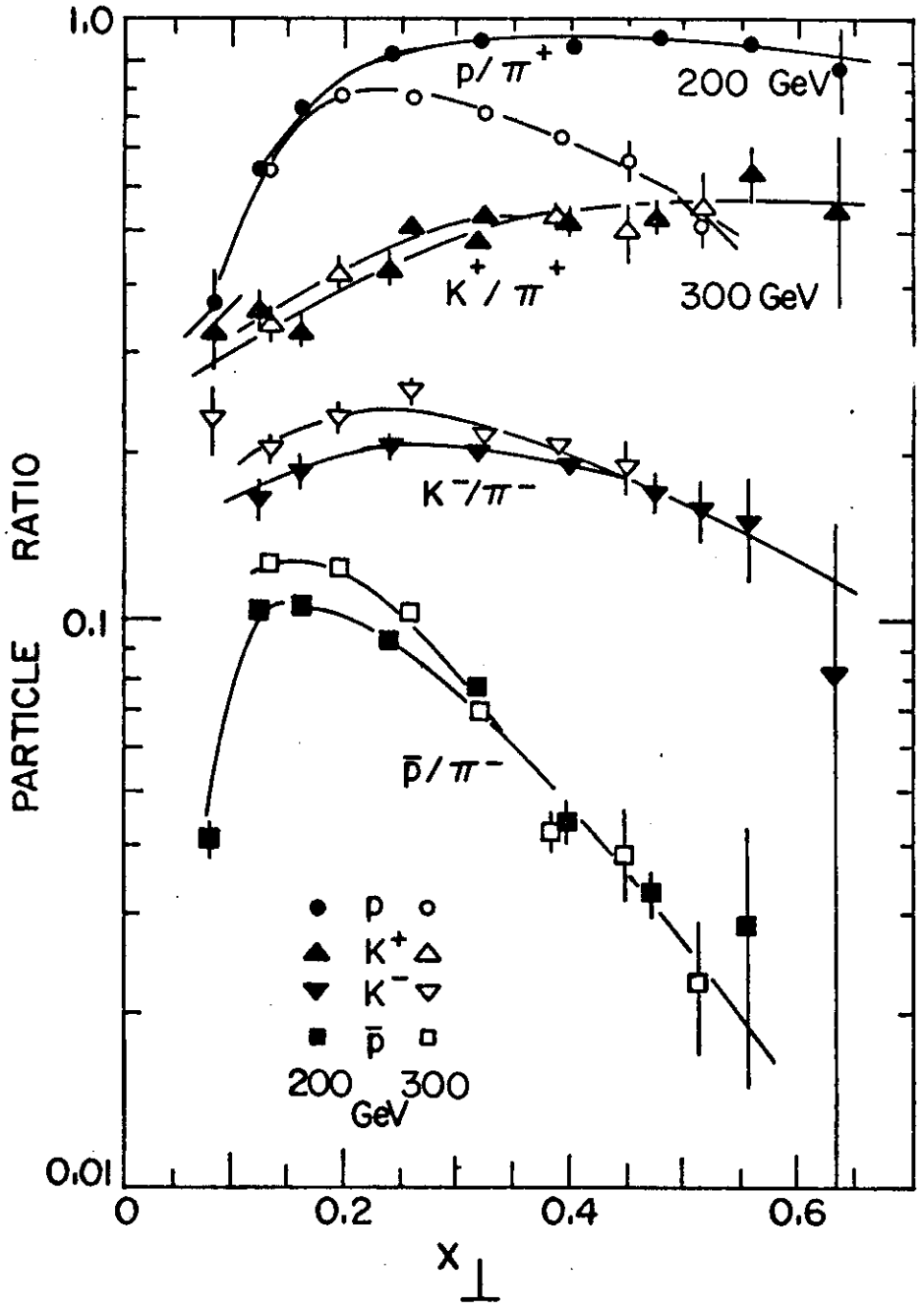
1.0
0.1
0.01
PARTICLE RATIO
p/π+
200 GeV
K+/π+
300 GeV
K−/π−
p̄/π−
p
K+
K−
p̄
200 300
GeV
0
0.2
0.4
0.6
X⊥

Fig. 15

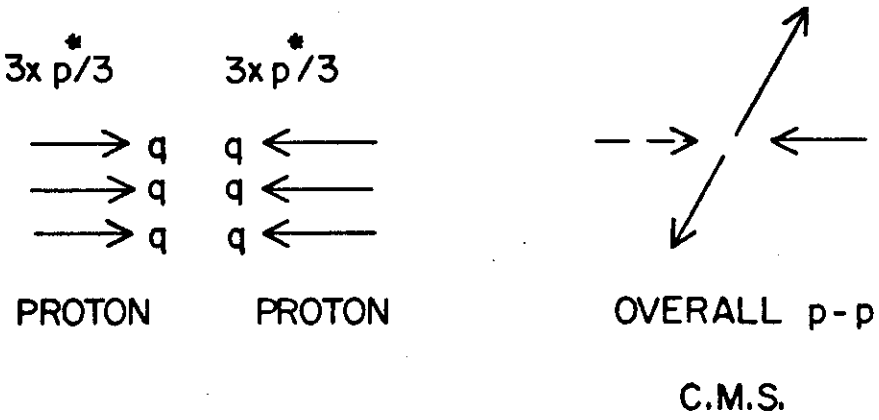
3x p*/3
3x p*/3
q
q
q
q
q
q
PROTON
PROTON
OVERALL p-p
C.M.S.

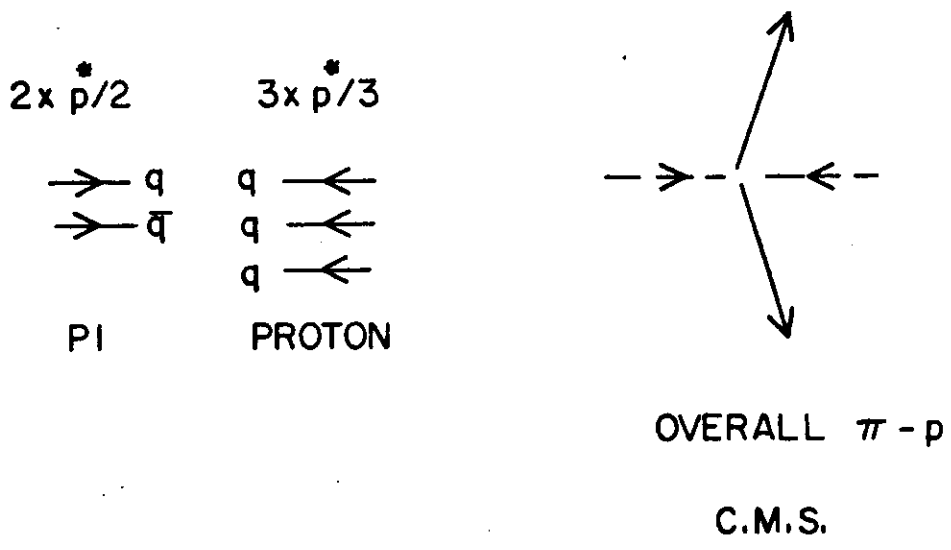
2x p*/2
3x p*/3
q
q̄
q
q
q
PI
PROTON
OVERALL π-p
C.M.S.

Fig. 16